ELSEVIER

Tectonophysics 320 (2000) 243–270

TECTONOPHYSICS

www.elsevier.com/locate/tecto

Indentation of a continent with a built-in thickness change: experiment and nature

Dimitrios Sokoutis [a,*], Marco Bonini [b], Sergei Medvedev [a,1], Mario Boccaletti [c], Christopher J. Talbot [a], Hemin Koyi [a]

[a] *Hans Ramberg Tectonic Laboratory, Institute of Earth Sciences, Uppsala University, Villavägen 16, 752 36 Uppsala, Sweden*
[b] *C.N.R. Analogue Modelling Laboratory — Centro di Studio di Geologia dell'Appennino e delle Catene Perimediterranee, via G. La Pira 4, 50121 Firenze, Italy*
[c] *Dipartimento di Scienze della Terra, Università degli Studi di Firenze, via G. La Pira 4, 50121 Firenze, Italy*

Abstract

Orogens oblique to the direction of plate convergence are currently attributed to obliquity between the margins of one or both of the sutured continents to their direction convergence. We use a single analogue experiment and natural examples to illustrate a potential additional factor: variations in strength of the indented continent at a high angle to the convergence direction. The wavelengths of structures in laterally shortened lithosphere depend on the strength of the most competent layers. Lateral variations in crustal thickness must therefore lead to structures oblique to any applied lateral compression.

An analogue experiment was performed to explore this phenomenon. A two-layer 'indented continent' was modelled by a brittle upper crust of sand above a lower crust of high-viscosity polymer floating on a single layer of low-viscosity syrup representing the mantle. The well-known strike-slip structures allowing lateral escape to distant weak boundaries were hindered by lateral boundaries in front of the indenter. This allowed us to focus on the effects of a thickness change built into the 'indented continent' along a zone parallel to the direction in which a vertical rigid wall advancing at a steady rate represented the indenter. Vertical escape led to an 'orogenic belt' oblique to the advancing wall; this obliquity influences subsequent lateral escape. Model scaling and interpretations are based on Extended Thin Sheet Approximation (ETSA) and standard theories of faulting.

Four sectors of the Alpine–Himalayan orogen (Iran, Tunisia, the Eastern Alps and the Himalaya) are oblique to the continental convergence direction, and we point to thickness changes at high angles to the suture that may account for this geometry. As crustal thicknesses north of oblique sectors of the Himalayas are not yet known, we speculate on them.

We infer from the main difference between our experiment and all our examples chosen from nature that vertical orogenic escape was oblique to our model suture but can be parallel to natural sutures.

Keywords: analogue modelling; Extended Thin Sheet Approximation (ETSA); indentation tectonics; lateral escape; oblique orogens; transversal crustal thickness variation

* Corresponding author. Present address: Aristotle University of Thessaloniki, School of Geology, Department of Geology and Physical Geography, 540 06 Thessaloniki, Greece. Tel.: +30-31-998512; fax: +30-31-998482.

[1] Present address: Geodynamics, Department of Oceanography, Dalhousie University, Halifax, NS, B3H 4J1, Canada.

E-mail address: sokoutis@geo.auth.gr (D. Sokoutis)

0040-1951/00/$ - see front matter
PII: S0040-1951(00)00043-3

1. Introduction

A few percipient geologists (Wegener, 1912; Argand, 1924; Carey, 1958) considered that large horizontal movements of continents were responsible for mountain belts long before the paradigm of plate tectonics convinced most geoscientists that orogens involve the subduction of ocean floor (McKenzie and Parker, 1967; Le Pichon, 1968; Morgan, 1968).

Subduction zones are more or less asymmetric in profile. This is because subducting oceanic lithosphere is cold, dense and stiff compared to the leading edge of the non-subducting plate that accretes weak sediments in a cold hydraulic arc. More material is transferred across plate boundaries involving the subduction of open oceans when magmas rising from the subducting oceanic plate arc weld the accreted prism of sediments into continental crust in either island or cordilleran arcs (Mitchel and Garson, 1976). Open-ocean subduction may be punctuated by the docking of small terrains with large continents. However, large persistent oceans can be closed by the suturing of continents and the development of new subduction zones elsewhere. The basic thermal and mechanical asymmetry of open-ocean subduction is carried over to the continental convergence that commonly follows ocean closure.

After continental suturing, mantle flow continues to drive the relatively cold and stiff continent on what had been the subducting plate into the continent warmed and weakened by the dying magmatic arc on what had been the non-subducting plate. Material continues to be transferred from one plate to another, but the direction of transfer before suturing is thought to be reversed after suturing. Instead of weak wet sediments being transferred from the subducting plate onto the non-subducting plate, continental suturing is thought to be followed by the transfer of weak warm upper crust onto cold stiff continent.

The transfer of sediments scraped off the subducting ocean floor into an accretionary prism on the non-subducting plate has been compared to Bulldozer tectonics (Davis et al., 1983). The post-suturing accretion of weak upper-crust onto the formerly subducting plate is an essential part of the process known as indentation tectonics (Backofen 1972; Tapponnier and Molnar, 1976). The use of two different mechanical models for accretion processes in different directions across the same plate boundary before and after suturing has obscured the essential similarity of these processes. We aim to answer the question to whether old inhereted changes in the thickness (strength) in the indented continent influence the map view of collisional orogens.

1.1. Previous models of the Alpine–Himalayan orogen

The dynamics of the Alpine–Himalayan orogen has previously been studied by several groups of analogue and numerical modellers.

Tapponnier and Molnar (1976) compared India to a rigid metal die or indenter driven into the weaker Asia that developed distinctive zones of plastic slip as a result. Indentation is usually treated in metallurgy as a two-dimensional symmetrical problem (where a die of finite width is driven into an infinite half-space). However, the first geological application was in 3D, and the results were described in terms of the tectonic escape of a weak indented thin crustal layer from a stiffer indenting continent. Thus, the rise along steep plastic thrusts of an orogenic belt along the leading edge of the indented continent was referred to as vertical tectonic escape. The development of distinctive patterns of strike-slip shear zones in the remote indented continent allowed what was called lateral tectonic escape.

Most previous studies of continental indentation tectonics focused on lateral escape. Large wedges of the indented continent rotate about vertical axes as they escape along curved paths toward a single asymmetric lateral boundary weakly constrained well beyond the face of the indenter. Thus, the northward indentation of Asia by India led to lateral escape of large wedges of Asia eastward toward subduction zones bounding the Pacific ocean (Tapponnier and Molnar, 1976; Tapponnier et al., 1982; Davy and Cobbold, 1988; Peltzer, 1988). Similarly, the indentation of Europe by a northward moving Adriatic indenter raised the Swiss Alps and, perhaps, the eastward escape

of the eastern Alps toward the subduction zone bounding the Carpathian arc (Ratschbacher et al., 1991a). Models by Faccenna et al. (1996) related the opening of the Tyrrhenian Sea to the northward indention by a rigid African plate. Regenauer-Lieb and Petit (1997) explained the Alps and associated zones of plastic shear in Central Europe by driving a sharp aluminium indenter representing the Italy–Adria block into a plastic 'Europe'.

Numerical experiments also help to improve our understanding of orogenesis (e.g. Burov, et al., 1993; Houseman and England, 1993; Royden, 1996; Sobouti and Arkani-Hamed, 1996). We will refer only to those works that are immediately relevant to our discussion.

The only initial thickness changes involved in previous studies were those between thick, laterally uniform continents and thin oceanic lithosphere. Here, we narrow the reference frame and restrict lateral escape (and associated rotation) by lateral walls in front of the indenter. This allows us to focus on the effect of changing the thickness (and therefore strength) of the indented continent along a line parallel to the convergence direction. The thickness changes that we built into the indented continent are 'pre-indentation' and equivalent to thickness changes inhereted from past plate tectonics, not those induced by indentation.

We start by describing a dynamically scaled analogue experiment and comment on its limitations before interpreting the results in terms of the interaction of different categories of forces. We investigate the interaction between body and boundary forces experimentally before applying our analysis to natural sectors of the Alpine–Himalayan mountain chain.

2. Experimental concept

The mountain chains of the Alpine–Himalayan orogen system (Fig. 1) are the result of northward migration of fragments of Gondwanaland and their suturing with Eurasia (e.g. Dewey et al., 1973, 1989; Biju-Duval et al., 1977; Tapponnier, 1977, 1978; Chase, 1978; Malinverno and Ryan, 1986; DeMets et al., 1990). The current convergence rate between Africa and Europe is approximately 1 cm/yr (Robbins et al., 1992; Ward, 1994), while that between Arabia and Asia is closer to 3.5 cm/yr (DeMets et al., 1990) and that between India and Asia is still between 3 and 5 cm/yr (Tapponnier, 1978). The Alpine–Himalayan orogen is generally close to perpendicular to the direction of current collision, but there are several sectors noticeably oblique to the first-order east-to-west trend (Fig. 1).

Structures associated with oblique orogenic sections suggested to us adjustment to lateral variations in the strength or thickness of the indented continent perpendicular to the convergence direction. We equate thickness with strength of the indented continent because we think in terms of old (pre-indentation) variations in thickness. Because these are inhereted from past plate tectonics, rather than new indentation, we do not anticipate any major differences in heat flow (e.g. Okaya et al., 1996). The seismic data indicate that a thicker crust is stronger than a thinner crust in the old indented continent. We therefore designed an experiment to explore such a phenomenon. This experiment had rigid lateral boundaries in front of the indenter to suppress lateral escape and emphasize vertical escape structures.

3. Experimental design

3.1. Model materials, boundaries and construction

The dimensions and orientations of zones that undergo vertical and lateral tectonic escape depend on the rheology and lateral boundary conditions of the indented and indenting plates (Gerbault et al., 1998). Understanding such processes, particularly at realistic deformation rates, depends largely on existing knowledge of the rheological properties of the lithosphere and asthenosphere (Davy and Cobbold, 1991 and references therein). This knowledge is based mainly on geophysical data and on extrapolating to lithospheric conditions the results of laboratory experiments at high pressures and temperature (Kirby, 1985; Carter and Tsenn, 1987; Ranalli and Murphy, 1987).

Assuming the lithosphere to be a brittle/ductile

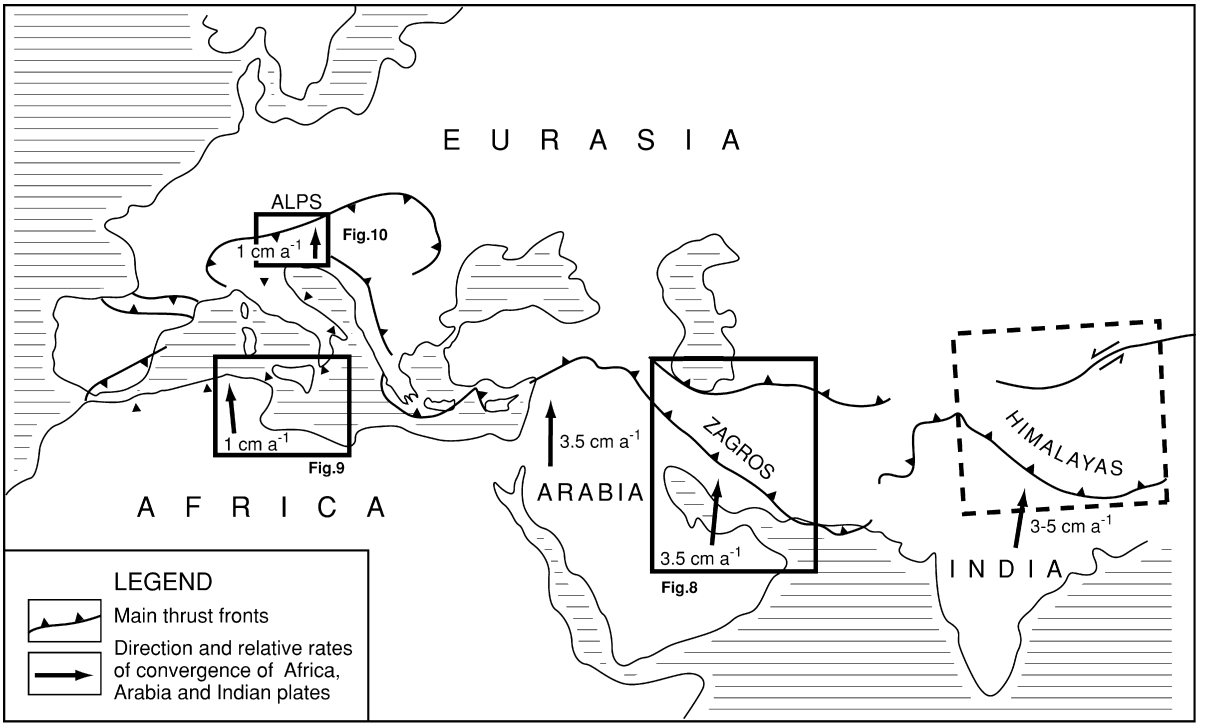

Fig. 1. Simplified tectonic map of the Alpine–Himalayan orogenic belt Numbered rectangles indicate orogenic sectors oblique to the convergence direction considered later.

multilayer system (e.g. Kirby, 1983; Ranalli, 1987; Ranalli and Murphy, 1987; Davy and Cobbold, 1991), analogue materials were employed to construct a three-layer model at the Hans Ramberg Tectonic Laboratory in the Department of Earth Sciences at Uppsala University. The upper two layers were competent and represented the upper brittle and lower ductile crust of the indented continent, and the lowest layer represented both the continental and asthenospheric mantle.

Dry sand, a Mohr–Coulomb material with density $\rho_u = 1300\ \mathrm{kg/m^3}$, negligible cohesion, and a coefficient of internal friction of 0.6, was used to simulate the brittle behaviour of the upper continental crust. The sand was sedimented in passive layers with different colours so as to visualize internal deformations. The ductile lower crust was simulated by a non-Newtonian layer produced by mixing finely ground barytes into SGM-36 type PDMS, a silicone putty with properties described by Weijermars (1986). This mixture has a density of $\rho_m = 1369\ \mathrm{kg/m^3}$ and behaves as a viscous fluid with a low power law exponent ($n < 1.5$) and effective viscosity of $\mu_d = (6 \pm 3) \times 10^5$ Pa s over the range of bulk strain rates in the experiment which lay between 1.3×10^{-5} and $2 \times 10^{-5}\ \mathrm{s^{-1}}$. This range is defined by the velocity of the moving wall divided by the instantaneous length of the model (see later).

The asthenosphere was simulated by a mixture of powdered gypsum in glycerol that resulted in a low-viscosity suspension with viscosity $\mu_a = 6$ Pa s and density $\rho_a = 1415\ \mathrm{kg/m^3}$. The deformation of the model and all the viscosity measurements were made in the temperature range of $24 \pm 2^\circ\mathrm{C}$. Instrumental limitations did not allow more exact rheological investigations, but our precision is sufficient for the analytical estimates and conclusions reported below.

The model was built in a Plexiglas box with dimensions $25 \times 38 \times 15$ cm (Fig. 2). The gypsum–glycerol 'mantle' was poured into the box and

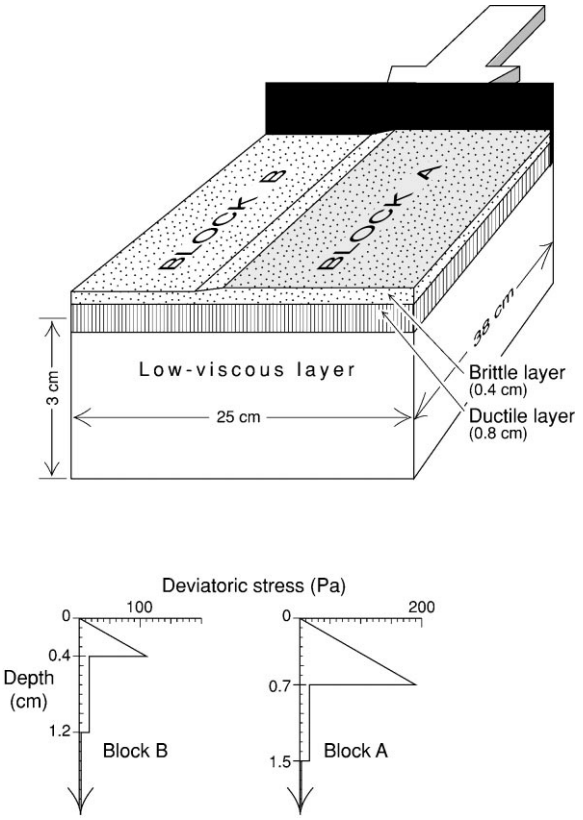

Fig. 2. Simplified sketch of the experimental apparatus and model construction. The strength profiles calculated for blocks A and B are based on the bulk strain rate of the experiment ($1.30 \times 10^{-5}\ s^{-1}$).

allowed to settle to a smooth 3 cm thick layer (Fig. 2). The PDMS + barytes layer simulating the ductile lower crust was then poured and allowed to settle to a constant thickness of 0.8 cm. The floating 'upper crust' of sand was then sedimented to a layer of constant 0.4 cm thickness. Half the box was then covered and left with a thickness of 0.4 cm (block B in Fig. 2), and continued sedimentation thickened the other half to a thickness of 0.7 cm (block A in Fig. 2).

The sand pack 'continent' with its built-in thickness change was then shortened along its length over an unshortened viscous 'mantle' using an electric motor to advance the proximal vertical Plexiglas wall at a constant rate of 1.8 cm/h up to 38% bulk shortening. Neither the floor nor any of the walls of the experimental box were lubricated, so they all acted as no-slip boundaries as expected in the natural examples considered later.

The no-slip boundary conditions along the floor, the three fixed walls and the single advancing wall define the external boundary forces acting on the model. The strengths of the model materials define the response to these forces throughout our layered analogue model. The strength profiles in Fig. 2 on either side of the thickness change are based on the initial bulk strain rate and illustrate the difference in strength between blocks A and B.

3.2. Isostatic compensation in the model

The initial lateral variations in thickness of the sand layer led to internal buoyancy forces that were stabilized by gravity driving isostatic adjustment. Following Ramberg (1968) and Artyushkov (1974), isostatic adjustment could be distinguished into three stages (Fig. 3 I–III). The first stage (loading) resulted in isostatic imbalance and gravity driving vertical movements of blocks A and B, which induced horizontal channel flow within the low-viscous 'mantle' (Fig. 3 I). This led to the second stage (Airy isostasy, Fig. 3 II) where the pressure along the bottom of the box was approximately constant (Turcotte and Schubert, 1982). The transition from the first to the second stage took several minutes in our analogue materials [see Appendix A, Eq. (6)]. Fig. 5 is thus idealized in the sense that the thickening of block B took longer than the time it could reach Airy Isostatic equilibrium. The transition between the second and third stage (total equilibrium: Fig. 3 III) took longer than the duration of the experiment. Hence, the predefined body forces in our experiment can be described by the transition from the second to the third stage of isostatic compensation (see Appendix A for details). The no-slip boundary conditions along the Plexiglas boundaries and the inhomogeneous thickening of the upper layers during lateral shortening further slowed down complete isostatic adjustment.

3.3. Simplifications in the model

The geometries and rheologies of analogue models simplify the complexities of nature to

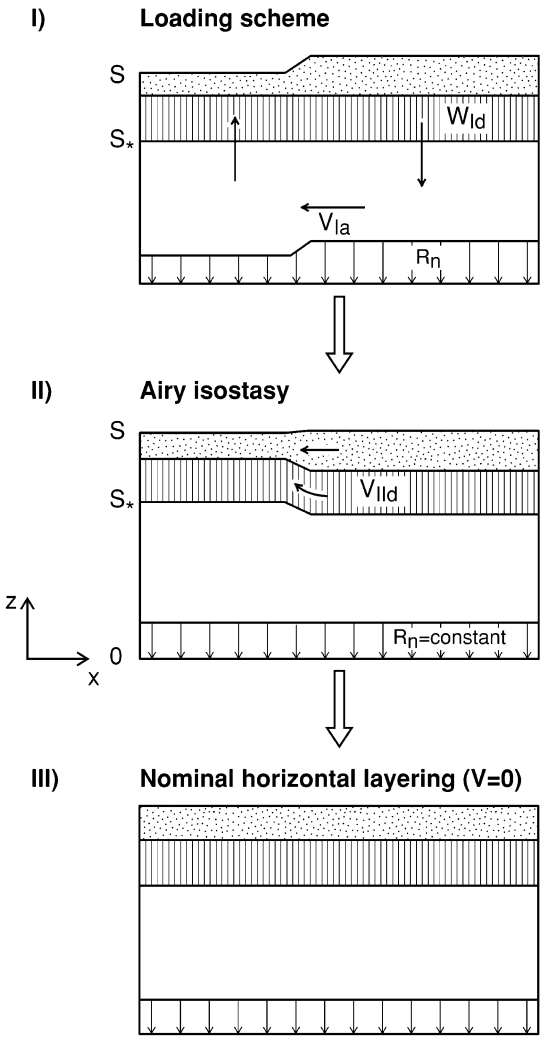

Fig. 3. Three sequential stages of isostatic adjustment. Note that these diagrams are idealized and do not take account of internal friction in the upper sand layer the final picture is likely idealized. See Appendix A for abbreviations.

resolve the process(es) under study. This section discusses some of the limitations of the simplifications that we made.

One type of simplification is usual in nearly all analogue experiments: the relations between the rheologies of the materials chosen as analogues of natural rocks. The properties of the lower crust are likely to be strongly temperature-dependent and therefore vary with depth. Representing the lower crust by a uniform isothermal layer of barytes mixed with silicone is a standardized simplification rationalized in detail by Davy and Cobbold (1988). We did not take account of the different modes of plastic behaviour of brittle materials that Buck (1997) recently emphasized may question modelling the brittle upper crust by cohesionless dry sand. This is because plastic shear in the continental crust may be localized snapping or distributed crunching while a sand layer mainly snaps.

The initial difference in thickness between upper sand blocks A and B was 0.3 cm across an experimental box 25 cm wide (resulting in a thickness ratio of $\sim 1/80$). This compares reasonably well with the natural examples considered later (e.g. a ratio of ~ 10 km/1000 km between the Iranian Plateau and the Lut block). None of the data concerning the properties of the upper mantle are of a comparable accuracy, and we assumed that the upper mantle deforms as a ductile material during orogenesis (e.g. fig. 8c in Cloetingh and Burov, 1996). Our experiment therefore represented both the upper (lithospheric) and lower (asthenospheric) mantle by a single low-viscous ductile layer and focussed on crustal deformation by shortening only the upper two layers of the model (Fig. 2). This is perhaps our greatest simplification of the natural situation where the whole lithosphere may take part in continent–continent convergence, at least in the Himalaya–Tibet system (Burov et al., 1993).

Our model also ignores natural recovery processes such as erosion, resedimentation or thermal readjustment. Thermal evolution is more easily followed by numerical models (e.g. Zhou and Sandiford, 1992; Genser et al., 1996), and we consider our analogue simulation as still useful despite this simplification.

The simplicity of our model allows definition of the influence of the fixed side walls so that we can neglect their influence when considering natural regions with rather weak lateral boundaries such as the Alps, Tunisia and the Himalaya–Tibet system (see later).

3.4. Scaling analysis

Our analogue experiment was generic rather than specific: it was designed to explore oblique

continental convergence in general, not to simulate any specific examples. Our scaling analysis comparing the experiment with selected natural examples can be divided into two parts that consider geometric and dynamic-rheological similarities (Weijermars and Schmeling, 1986).

Geometrical similarity is defined by ϵ, the ratio between the thickness and the horizontal length scale of the crust, and the results are presented in Table 1. Although the scaling looks suspect beacause we (necessarily) compare the 'pre-deformation' model with post orogenic prototypes in nature, the significant thicknesses changes in the indented continent are inhereted from previous events and therefore also pre-date the deformation that we model.

The rheological simplifications of the analogue model and the lack of data concerning natural rheological stratification offer a route for checking dynamic similarity by dimensional analysis. Following Weijermars and Schmeling (1986), we start by assuming a dynamic similarity between the model and natural examples and then use the Ramberg number, *Rm*, as a measure of this similarity. The Ramberg number represents the ratio of gravitational to viscous forces acting in a system:

$$Rm_{\text{experimental}} = \frac{\rho g h_{\text{d}} L|}{\mu_{\alpha} V_{\text{c}}|_{\text{experimental}}} \sim 50 \approx Rm_{\text{natural}}$$

(see Table 1 for definitions of symbols).

We assume that *Rm* in our natural examples is equal to that in the experiment and then estimate the mean bulk viscosity of the natural lower crust for each area. The viscosities estimated for the lower crust (Table 1) are sufficiently similar to those used by other workers to justify our initial assumption of dynamic similarity between our experiment and natural examples because they share similar Ramberg numbers. As the natural and experimental upper crusts share similar parameters of brittle behaviour, we can extrapolate our conclusion of dynamic similarity to the whole crust.

4. Results of experiment

To simplify descriptions of successive stages during the progressive deformation of the experiment in plan view, we refer to the advancing wall as proximal and the fixed wall beyond as distal (Fig. 4a). The proximal advancing wall represents the cold indenting continent during continental convergence, and its front face represents the suture. We describe the sequence in which the structures develop before presenting an integrated picture (Fig. 5). It will be useful to distinguish belts of deformation structures and intervening domains on particular blocks. Domains are labelled by the initial block in which they develop while the belts are numbered according to the time sequence in which they develop. The built-in boundary between blocks A and B will be referred throughout as the 'Δ belt' (from the Greek 'Διαιρω', which means divide).

At 2% bulk shortening (% BS), the first structure to form was a fore thrust that surfaced 1 cm in front of the moving wall across block A (Fig. 4b). Soon after, a back thrust also crossed block B close to the mobile wall.

Table 1
Scaling parameters of the experiment and natural examples

	Experiment	Zagros	Tunisia	Alps	Tibet
Thickness of crust, h_{c}					
Maximum	1.5 cm	60 km	40–45 km	50 km	80 km (?)
Maximum	1.3	40 km	25–25 km	30 km	60 km (?)
Horizontal scale, L	25 cm	900 km	400 km	100×300 km	1500 km
$\epsilon = h_{\text{c}}/L$	5.5×10^{-2}	5.5×10^{-2}	$8–10 \times 10^{-2}$	13×10^{-2}	4.7×10^{-2}
Collision rate, V_{c}	1.8 cm/h	3.5 cm/yr	1 cm/yr	1 cm/yr	5 cm/yr
Effective viscosity of the lower crust $\mu_{\text{d}} = \rho g h_{\text{d}} L (Rm V_{\text{c}})^{-1}$	5×10^{5} Pa · s	10^{22} Pa · s	10^{23} Pa · s	10^{23} Pa · s	2×10^{22} Pa · s

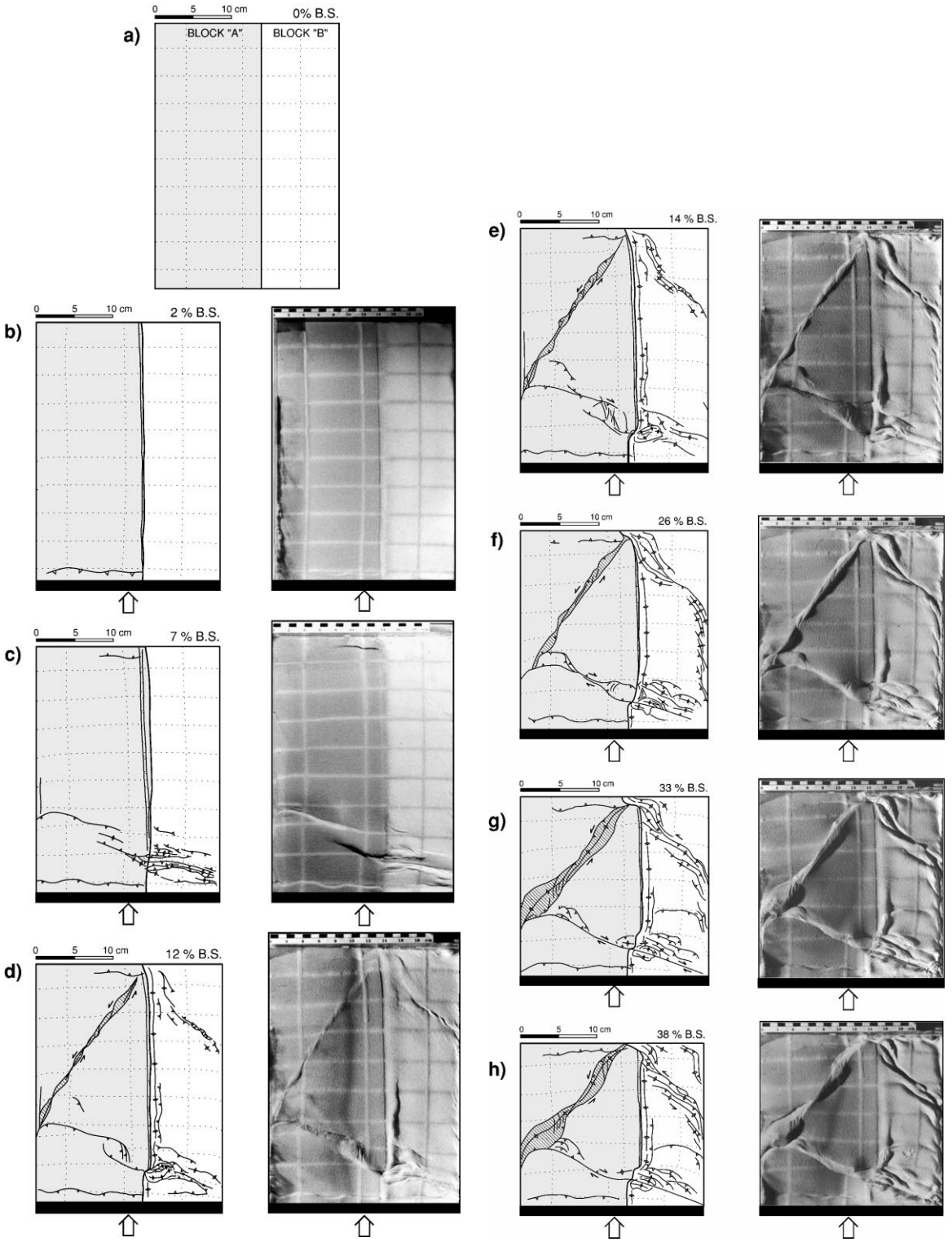

Fig. 4. Right column: top-view photos of model at particular stages. Left column: interpretative line drawings of the experiment.

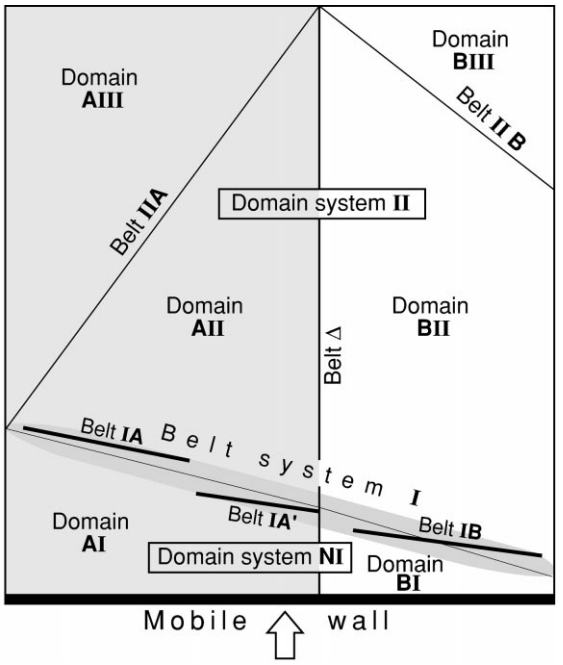

Fig. 5. Simplified cumulative map of domains of low deformation separated by highly deformed belts. The arrow indicates the direction of convergence.

After 7% BS (Fig. 4c) deformation within the model was inhomogeneous and belts of en-echelon box-folds bound by both fore- and back thrusts began to develop (IA, IA′, IB in Fig. 5). Distortion of a marker line along the edge of the thinner block (B) indicated that the thicker block (A) bulged over the thinner block in profile. Partial accommodation of this lateral escape of block A toward block B was indicated by a strong component of dextral shear offsetting marker lines crossing the fore thrust closest to the inner edge of Block A (belt IA′ in Fig. 5). Less significant lateral shear occurred along belt IA, and none is obvious along the closer-spaced structures in belt IB (Fig. 4c). The end of this early stage of deformation was marked by the surfacing of a back thrust across the distal part of block A indicating that strain had propagated the complete length of block A.

At about 10% BS, while the box folds in belt system I tightened, a new belt of left-lateral transpressive shear (belt IIA on Fig. 5) rapidly propagated diagonally and distally across block A from the left hand end of belt system I to where the Δ belt met the fixed distal wall (Fig. 4d). Offsets of marker lines indicate that the triangular domain of block A (domain AII in Fig. 5) laterally escaped asymmetrically toward block B in a direction parallel to belt IIA without any noticeable internal deformation. This oblique expulsion of block AII generated a new diagonal belt of en-echelon thrusts (IIB in Fig. 5) across the distal right corner of block B (Fig. 4d). By 12% BS, the lateral escape of block AII was most pronounced where thrusts in domain BII dipped beneath the proximal half of the leading edge of block A and near the distal wall (Fig. 4d).

The major components of the structural pattern evident at the end of the experiment (after 38% BS) were already clear by about 12% BS. Thereafter, all existing structures merely became more pronounced. During the intermediate stages of shortening (from 7 to 26% BS), belt system I progressively narrowed and straightened to a zone diagonal across both blocks from the proximal right hand corner to the distal tip of domain AII (Fig. 4e).

During the final stage of shortening (from 26 to 38% BS) most of the deformation occurred along belt system I, while the other pre-existing structures simply became progressively more pronounced (Fig. 4e–h). The exception was belt IIA, along which early zones of mainly strike-slip faults developed into a belt of mainly thrusts. Cross-sections (Fig. 6a–g) illustrate where the sand layer thickened by thrusting.

Progressive deformation in the experiment can be divided into three stages illustrated by a plot of relative movements of three reference points (Fig. 7):

(1) The first stage (0–10% BS) was characterized mainly by local vertical escape. The rapid advance of reference point 1 (Fig. 7) was a result of box folds bound by fore- and back thrusts (in belts IA, IA′, IB) developing just in front of the advancing wall. This stage was terminated by the appearance of thrusts along the Δ belt and the initiation of shear belt IIA.

(2) The second stage (12–26% BS) was marked by deformation propagating throughout the model and lateral escape. The fast motion of point 2

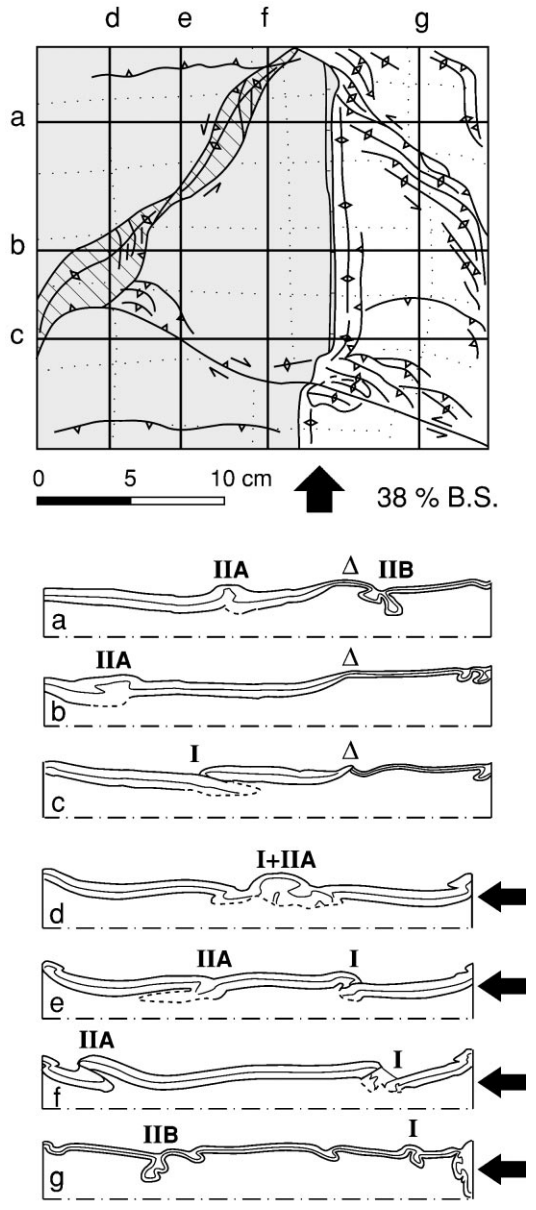

Fig. 6. Cross-sections after the experiment had been terminated: a–c are perpendicular to the shortening direction, d–g are along the shortening direction.

(Fig. 7) indicates that lateral escape involved mainly translation of domain AII along the right-lateral shear belt IIA. The contemporaneous deceleration of point 1 (relative to stage 1) was because thrust belts IA, IA′, and IB joined to form thrust belt system I with a low component of strike-slip displacement.

(3) A change in the relative direction of motion of point 3 (Fig. 7) signalled the third stage of deformation (26–38% BS) when lateral escape of domain AII along belt IIA stopped because of development of thrust belt IIB. After about 26% BS, the model merely deformed along pre-existing structures. The lateral escape during this stage was driven mainly by gravitational spreading, which is indicated by no significant changes in the rates of motion of points 1 and 2 and further development of bulging along Δ belt in profile.

Acceleration in the progressive advance of point 2 (Fig. 7) indicates that belt IIA and domain AII were rotated by bulk shortening during both the second and third stages.

5. Interpretation of dynamics in experiment

The localization of deformation to narrow belts until 26% BS indicates that the style of deformation was dictated by snapping of the upper brittle sand layer during the first two stages of shortening. None the less, the influence of the ductile layers throughout the initial stages can be recognized by two features: (1) once initiated, faults in the sand layer accumulated strain continuously throughout the progressive shortening; and (2) slow continuous isostatic adjustment results in bulging along the Δ belt (Fig. 4a–c) in profile, lateral extension across block A and lateral compression across block B.

Shortening due to the advance of the mobile wall resulted in box folds. Two sets of folds with different wavelengths and amplitudes could be distinguished in the first stage of deformation, up to 7% BS (Fig. 4c). These differences can be attributed to the differences in competence of the two adjacent blocks due to their initial differences in thickness. The most competent layer in the model, the sand (Fig. 2), defines the wavelength of folding. Because the sand in Block A was almost twice as thick as that in Block B, box folds across block A developed with a wavelength almost twice that across Block B.

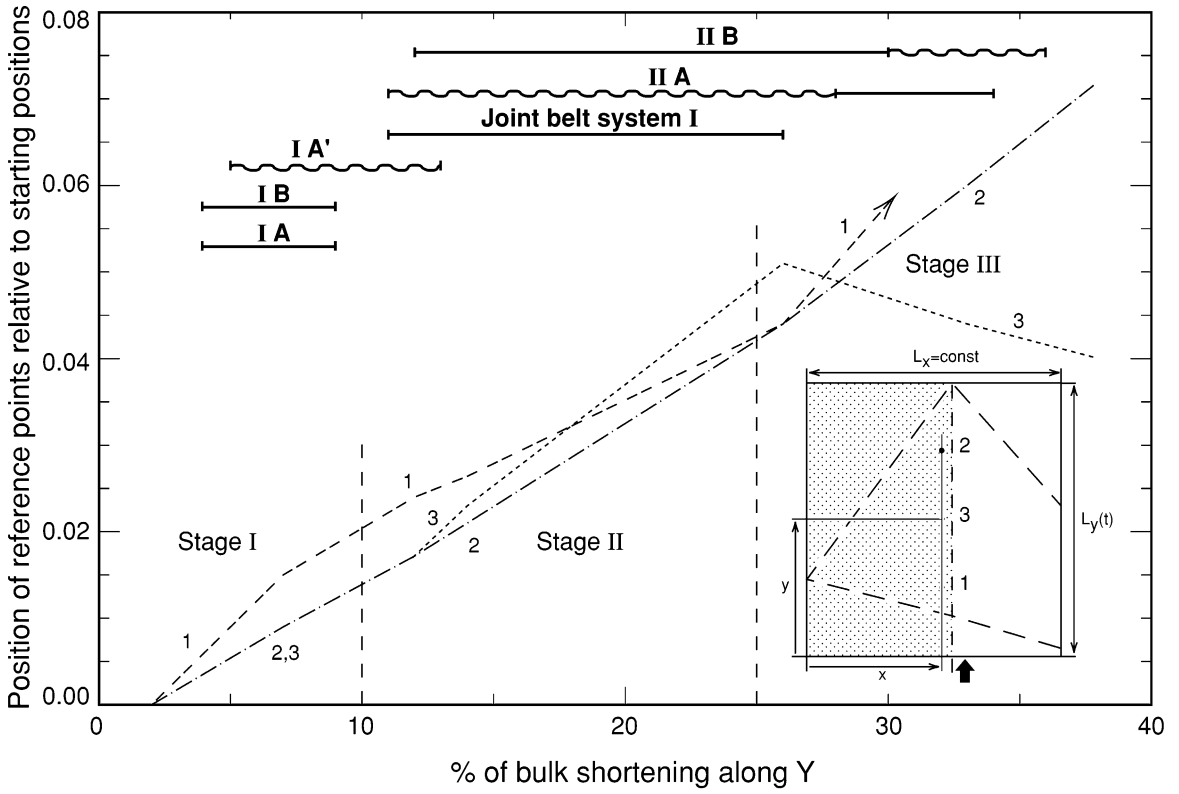

Fig. 7. Positions of reference points relative to initial fixed within domain AII. Their different rates of motion allow subdivision of the sequential deformations into three stages. Relative horizontal positions of points 1 and 2 are calculated using formula $(x-x_0)/L_x$, and the vertical positions of point 3 are calculated using formula $[y_0/\ L_y(0)-y/L_y(t)]$. Index 0 denotes the initial position of points (at 2% of BS), and the remaining parameters are cartooned. The relative motion of points 1 and 2 clearly demonstrate right-directed motion across the Δ belt. The positive position of point 3 indicates that deformations in the region between this point and moving wall accommodate more shortening than more distal parts. Note that although the absolute motion of reference point 3 is always toward the distal boundary, its relative motion reverses because of changes in the referent length $L_y(t)$ (see stage III). Reference point 1 was involved in thrusting and could not be measured during stage III. The main stages of evolution of the fault belts are distinguished into wavy lines (mainly strike-slip) and straight lines (mainly thrusts) at the top of the diagram.

The distribution of stresses within blocks A and B was subject to the boundary conditions imposed by both the fixed and moving walls. Thrusts developed in belts IA and IB because the maximal principal stress was along the direction of shortening, and the minimum was vertical (Davy and Cobbold, 1991). The stress distribution differed across the Δ belt. The horizontal stress orthogonal to the Δ belt in block A near the Δ belt was decreased by isostatic adjustment towards block B. Both the maximum and minimum principal stresses approached the horizontal in this region. This resulted in a thrust fault with a high strike-slip component, IA′, propagating from the Δ belt inside the block A (Fig. 4c). The development of fault IA′ is indicated by the fast motion of reference point 1 (Fig. 7) and by the bulging in profile converting into a thrust in the adjacent part of the Δ belt at an early stage.

As shortening progressed, early strike-slip displacements decreased along the faults in belt IA, IB and IA′ (Fig. 4d–e), which straightened and, at about 20% BS, merged into a single continuous system of thrusts (belt system I on Fig. 5). Belt system I was oblique to the advancing wall representing the suture zone, and we use its continuity

to define domain system NI (Fig. 5), which is a combination of domains AI and BI. Comparisons between deformation at various stages (on Fig. 4f–h) demonstrate that domain system NI underwent essentially no internal deformation after about 20% BS. A later discussion will refer to indented material as having been transferred across Belt system I onto the advancing indenter so that all subsequent deformation was distal. The sand transferred (domain system NI, Fig. 5) thereafter advanced as a rigid forward extension of the wall acting as the initial indenter. Since we did not induce this effect, we will refer to domain system NI (Fig. 5) as an *effective indenter* added to the initial indenter.

The second structure to form in block A, belt IIA (Fig. 5), developed between the left-hand end of the front of the effective indenter and the distal end of the Δ belt. As in the genesis of belt IA′, as soon as bulk shortening had established a zone of adjustment across the Δ belt, both the maximum and minimum principal stresses approached the horizontal. This activated the strike-slip faults in belt IIA, and the geometry of belt IIA was influenced by the size of the experimental box compared to the fold wavelength in block A. Strike-slip shear along Belt IIA localized lateral shear stresses induced by the left-hand and distal walls and isolated domain AIII from the gravity spreading of domain AII (cf. discussion and results of experiments in Davy and Cobbold, 1991).

The development of strike-slip belt IIA allowed distal translation of domain AII along belt IIA resulting in thrusting in belt IIB across the corner of block B. Thus, belt IIB is the result of the lateral escape of domain AII. This explains the low deformations in the centre of block B despite its weakness. The shorter wavelengths of thrusts dispersed along block B were isolated by shear along the fixed wall from thrusting along belt IIB across the distal corner of block B.

As deformations continued, belt IIB developed so that strains accumulating in domain BII restricted further lateral motion of domain AII. This raised the horizontal stresses above the vertical stress so that belt IIA transformed from a zone of mainly left-lateral strike slip into one of thrusts as the second stage of model deformation became the third (Fig. 4f–g).

The relative position of point 3 indicates that belt system I was the most active throughout the deformations. However, the negative slope in the relative changes in position of point 3 during the third stage (Fig. 7) indicates that the deformation then became more homogeneous throughout the model. In general, deformations of the third stage were characterized by all belts converting the advance of the indenter into oblique thrusts.

First-stage vertical escape near the advancing wall led to second stage lateral escape, which was restricted by the lateral boundaries, leading to the reappearance of vertical escape in the third stage.

Cross-sections of the model (Fig. 6d–g) demonstrate the different styles of deformations in blocks A and B (see also Cobbold et al., 1995, where changes in thickness of the stiff layer were along the direction of shortening). The thicker sand layer (block A) was shortened mainly by box anticlines bound by thrusts. By contrast, the thinner sand layer (block B) was shortened mainly by being depressed into its ductile substrate along box synclines (the 'pop-downs' of Cobbold et al., 1995). The upward escape of the thicker sand and the downward escape of the thinner sand reflect the relative strengths of the brittle and ductile layers. Unfaulted, the sand layers in both blocks are stronger than the underlying ductile layer (Fig. 2). Faulting lowers the strength of the sand layer significantly (by approximately 80%; Vermeer, 1990). Where the thin sand layer is faulted, it appears to be of a similar effective strength to the underlying ductile layers. Progressive thickening of the sand in the thinner block (B) occurs in local tight synclines (Fig. 6g). By contrast, the thicker block (A) remained much stronger than the viscous layer and always shortened by much wider box anticlines (Fig. 6d–f). The late-stage dynamics were influenced by the sand in domain AII doubling in thickness, while the sand layer in domain BII generally retained its original thickness.

Isostatic adjustment between domains AII and BII extended domain AII and shortened BII perpendicular to the shortening direction throughout the experiment. The different styles of thickening in blocks A and B accelerated gravity spreading

during the later stages of shortening to a rate that can be estimated using Eq. (8) from Appendix A. The initial difference in thickness across the sand layer, Δ_h, was tripled and implies a rate of spreading in close agreement with direct experimental measurements ($\sim$0.3 cm/h). Cross-sections across the direction of shortening (Fig. 6a–c) indicate significant deformations at the base of the sand layer near the Δ belt. This supports the assumptions made in Appendix A that the most active force perpendicular to the direction of shortening is the isostatic adjustment driven by viscous layers.

6. Natural examples

6.1. Zagros mountains–Iranian plateau and Lut block system

The Iranian plateau is located in the convergence zone between the Arabian and Eurasian plates. Suturing between Arabia and Iran began in late Miocene at an approximate rate of 3.5 cm/yr (DeMets et al., 1990; Fig. 8). Focal mechanism solutions for earthquakes in the region indicate that convergence between these two plates is still active in a nearly N–S direction (Jackson and McKenzie, 1984). Most of the convergence is accommodated by crustal thickening and consequent uplift of the Iranian plateau and deformation along its boundaries (Berberian, 1981; Sobouti and Arkani-Hamed, 1996). Most of the bulk crustal shortening associated with this plate convergence probably occurs across the most active seismic zone in Iran, along the NW–SE-trending Zagros mountain chain. This chain is markedly oblique to the almost N–S direction of plate convergence and fault-plane solutions, and field evidence indicates a dextral strike-slip component of displacement along the belt (Tchalenko and Braud, 1974; Berberian, 1981; Jackson and Fitch, 1981; Jackson and McKenzie, 1984, Jackson and McKenzie, 1988; Alavi, 1992). The Zagros and the central Iranian plateau are separated from the Makran subduction zone by the N–S-trending Nayband fault zone bounding the western edge of the Lut block (Fig. 8).

Central Iran is characterized by a major conjugate fault system consisting of two major fault zones: sinistral shear along the NE trend of the Great Kavir fault is associated with southeast-directed thrusting in the north, while dextral shear is recorded along the NW-trending Naiin fault in the south (Fig. 8). These dynamics transfer material eastward the Lut block squeezing the numerous salt diapirs along the western boundary of the Lut block that are elongated along the N–S-trending Tabas–Kerman alignment, (Fig. 8). The Lut block is rectangular in shape and bounded by the dextral N–S-striking Nehbandan fault belt to the east, the dextral Nayband fault belt to the west, the sinistral Great Kavir fault to the north and the Makran subduction zone to the south (Fig. 8). The Zagros–Iranian plateau and Lut block system are bounded to the north by the S-verging Elburz–Kopet Dagh fold-thrust belt (Fig. 8 and Alavi, 1992).

Gravity modelling indicates that the crustal thickness increases from 40 km along the SW edge of the Zagros mountains up to 58–65 km beneath the main thrust belt (Snyder and Barazangi, 1986). Seismic refraction data (Giese et al., 1983) indicate a crustal thickness of about 55–60 km in the Zagros mountains. Tomographic modelling indicates a crustal thickness greater than 50 km for the Iranian plateau (Central Iran; Hearn and Ni, 1994), whereas the crustal thickness of the adjacent Lut block has been estimated at less than 40 km (Dehghani and Makris, 1983; Sobouti and Arkani-Hamed, 1996). This crustal configuration includes a lateral variation in crustal thicknesses that is perpendicular to the regional direction of shortening. Thus, the Iranian Plateau is similar to Block A in our experiment, and the Lut block is similar to Block B.

6.2. Tell–Atlas and Pelagian block

In contrast with the other examples, the Tunisian–Pelagian blocks are part of the African foreland south of the main thrust front of the Alpine–Himalayan orogenic system (Fig. 1). In terms of indentation tectonics, the Tunisian–Pelagian region may be considered as indented by the cold block north of the Tell chain moving relatively southward (Fig. 9). Other structural

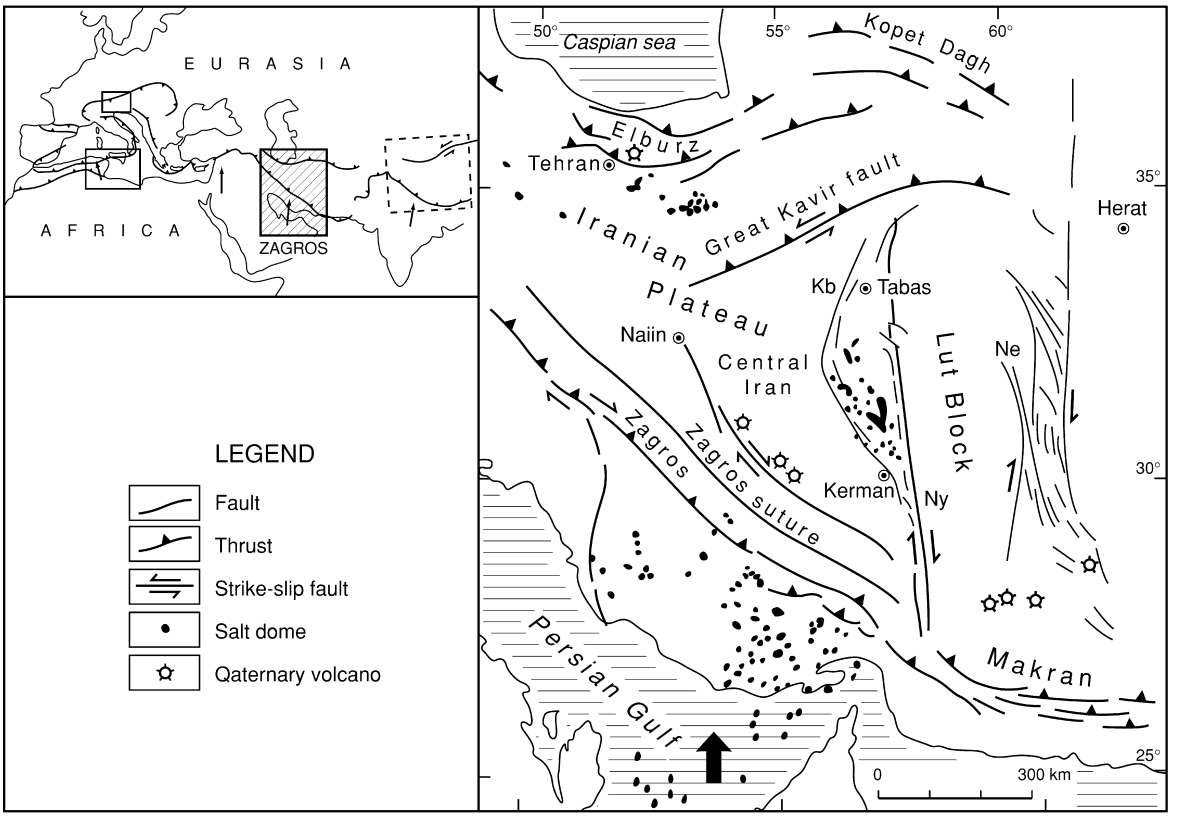

Fig. 8. Tectonic sketch map of Iran (simplified from Jackson et al., 1990). Kb: Kuh-Banan fault belt; Ny: Nayband fault belt; Ne: Nehbandan fault belt.

components dividing this sector into blocks include the W–E-trending Sahara Atlas chain to the south, the North–South Axis belt (NOSA) separating the Pelagian block in the east from Tunisia in the west, and the NW–SE-trending Gafsa belt in the south west (Fig. 9).

The Tell thrust belt consists of a pile of mainly south-verging tectonic units that resulted from the suturing between the rifted northern margin of the African plate moving northward into the European plate (e.g. Dewey et al., 1989). The Tell thrust and fold belt extends eastward from northern Tunisia to the offshore Straits of Sardinia. Thrusting began in the Tell in late Oligocene times (Snocke et al., 1988) but most of the chain formed during the Middle Miocene (Rouvier, 1977) and underwent alternating compressional and extensional throughout Miocene to Pleistocene (Rouvier, 1977; Cohen et al., 1980; Zargouni and Abbés, 1985; Boccaletti et al., 1990).

The Atlas chain has been interpreted as a Middle Miocene fold belt without any major thrusts (Boccaletti et al., 1990), whereas Snocke et al. (1988) related the folds to inversion of NE–SW-trending syn-rift basement faults. However, seismic line interpretation (e.g. Hlaiem et al., 1997) indicates that the southern front of the Atlas is marked by N-dipping reverse faults.

The eastern boundary of the Atlas mountains, the so-called North–South Axis (NOSA), has been interpreted as either the front of a collision-related thin-skinned thrust-fold belt (Truillet et al., 1981; Anderson, 1996), or as a sinistral positive flower structure related to the reactivation of a deep-seated basement discontinuity (Philip et al., 1986; Ouali et al., 1987; Boccaletti et al., 1988, 1990).

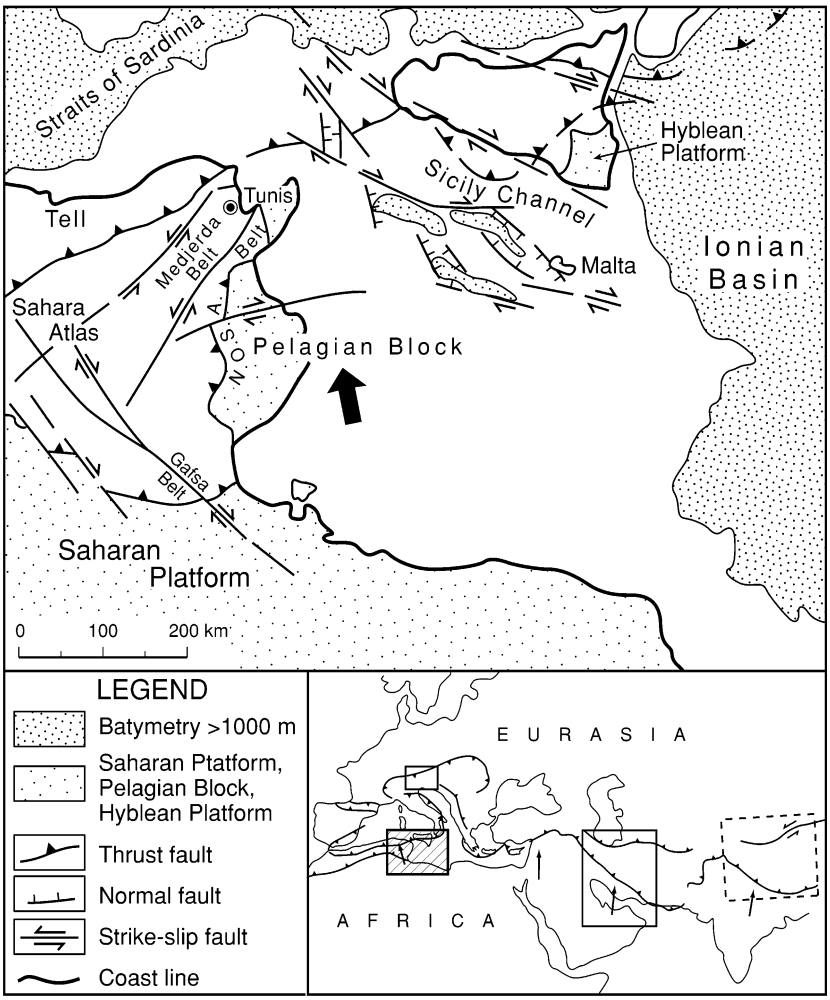

Fig. 9. Tectonic sketch map of Tunisia and Central Mediterranean (compiled from Boccaletti and Dainelli, 1982; Boccaletti et al., 1982, 1984, 1985, 1987, 1988, 1990; Anderson, 1996).

Reactivation of basement faults has also been suggested for both the Gafsa belt (Boccaletti and Dainelli, 1982; Boccaletti et al., 1982, 1987; Anderson, 1996) and the NE–SW Medjerda trend (Boccaletti and Dainelli, 1982; Boccaletti et al., 1982, 1984; Snocke et al., 1988) that together represent conjugate fault sets affecting the Atlas chain (Fig. 1). The age of deformation in the NOSA belt is still controversial since Boccaletti et al. (1990) suggest a Late Miocene–Pliocene age while Anderson (1996) suggests Middle Miocene.

The Gafsa belt is characterized by large dextral strike-slip movements (Zargouni, 1984), whereas the Medjeda belt is characterized by large mainly left-lateral, strike-slip displacements (Boccaletti and Dainelli, 1982; Boccaletti et al., 1982, 1987). These two strike-slip fault belts form a conjugate system that generated the Atlasic pull-apart basins (Boccaletti et al., 1985, 1990; Philip et al., 1986) and extruded the Atlas eastward over the Pelagian Block. Deformations in both the Gafsa and Medjerda belts are referred mainly to Late Miocene–Pleistocene times (Boccaletti et al., 1987, 1990), in which case, they were coeval with thrusting in the NOSA belt (Boccaletti et al., 1987, 1990, but see Anderson, 1996). A wider time range

(Early Miocene to Pleistocene) has been suggested for the development of the Atlasic pull-apart basins by Philip et al. (1986).

Deep seismic sounding data (Zargouni and Abbés, 1985) indicate that the crust is 40–45 km thick beneath the Tell–Atlas mountains (see fig. 3 in Boccaletti et al., 1990), while the crustal thickness is between 25 and 35 km in the adjacent Pelagian block to the east (Cassinis, 1983). Inverting the map (Fig. 9) produces a crustal configuration reminiscent of the final stage of our experiment.

6.3. Eastern Alps

The Alps represent one of the most spectacular orogenic belts in the world. This orogen is attributed to N–NNW-directed convergence between the cold Adriatic plate and the warm European plate (Fig. 10a). The weak margin of European crust was thickened during Eocene–Neogene during indentation by the stiff Adriatic plate (Tapponnier, 1977; Ratschbacher et al., 1991a,b; Regenauer-Lieb, 1996; Schmidt et al., 1996).

Collision and subsequent convergence involved northward thrusting and southward back thrusting of a wedge of European upper crust onto the Adriatic crust along the Periadriatic Line with a dextral transpressive component (Fig. 10 after Schmidt et al., 1989, 1996; Pfiffner et al., 1990, and references therein). The first-order structures have been attributed to vertical extrusion followed by extensional collapse due to gravity spreading (Dewey, 1988) together with lateral escape of the eastern Alps eastward toward the Pannonian basin away from the N or NW crustal shortening across the Swiss Alps (Ratschbacher et al., 1991b). Eastward escape would have been favoured by the continental crust of the Eastern Alps having decoupled from the mantle (Burov and Diament, 1995) and a weak lateral boundary to the east (Tapponnier, 1977; Burchfiel and Royden, 1982; Royden et al., 1983; Balla, 1985; Ratschbacher et al., 1991a,b). Eastward escape was accommodated by an array of conjugate ESE- and ENE-trending strike-slip faults in front and to the east of the Adriatic indenter (Fig. 10a).

The Alpine orogenic crust is over 50 km thick at the Tauern window and thins eastward to less than 30 km under the western margin of the Pannonian basin (Müller et al., 1980; Giese et al., 1982). The Alpine crust in front of the Adriatic indenter is therefore generally thicker to the west of the Lavantal fault zone and thinner to the east (Fig. 10b, after Ratschbacher et al., 1991b). If a similar change in crustal thickness extends orthogonal to the regional direction of shortening north of the Alps, the crustal configuration is similar to our experiment.

7. Discussion

Pre-collision changes in thickness in what later become indented continents can arise in numerous ways. In Iran, the Lut block may have been an exotic terrain inserted into the system during early Miocene (Talbot and Alavi, 1996). Similarly, the Pelagian block may have been added to Tunisia rather recently. We know of no obvious pre-orogenic lateral variations in the strength of Europe in front of the Eastern Alps or of Asia in front of the Himalaya–Tibet systems.

7.1. Effective indenters in vertical and horizontal escape

The effective indenter is not a unique feature of our work and there are several types.

Recent work at Uppsala has systematically explored how the geometry of the indenter effects vertical tectonic escape in profile (Bonini et al., 1999; Persson, submitted for publication). Rigid indenters with front faces having different dips were driven into sand packs with passive colour markers to study the vertical escape process in profile. The only case where the initial indenter continues to act as the effective indenters is that where the dip of the rigid front face coincides with the angle of internal friction of the indented material ($30 \pm 15^{\circ}$). In this case, vertical escape occurs by the rise of a triangular orogenic wedge between a series of fore thrusts in the sand and the front face of the rigid indenter (Persson, submitted for publication). In what must presumably be the general case, where the front face of the rigid

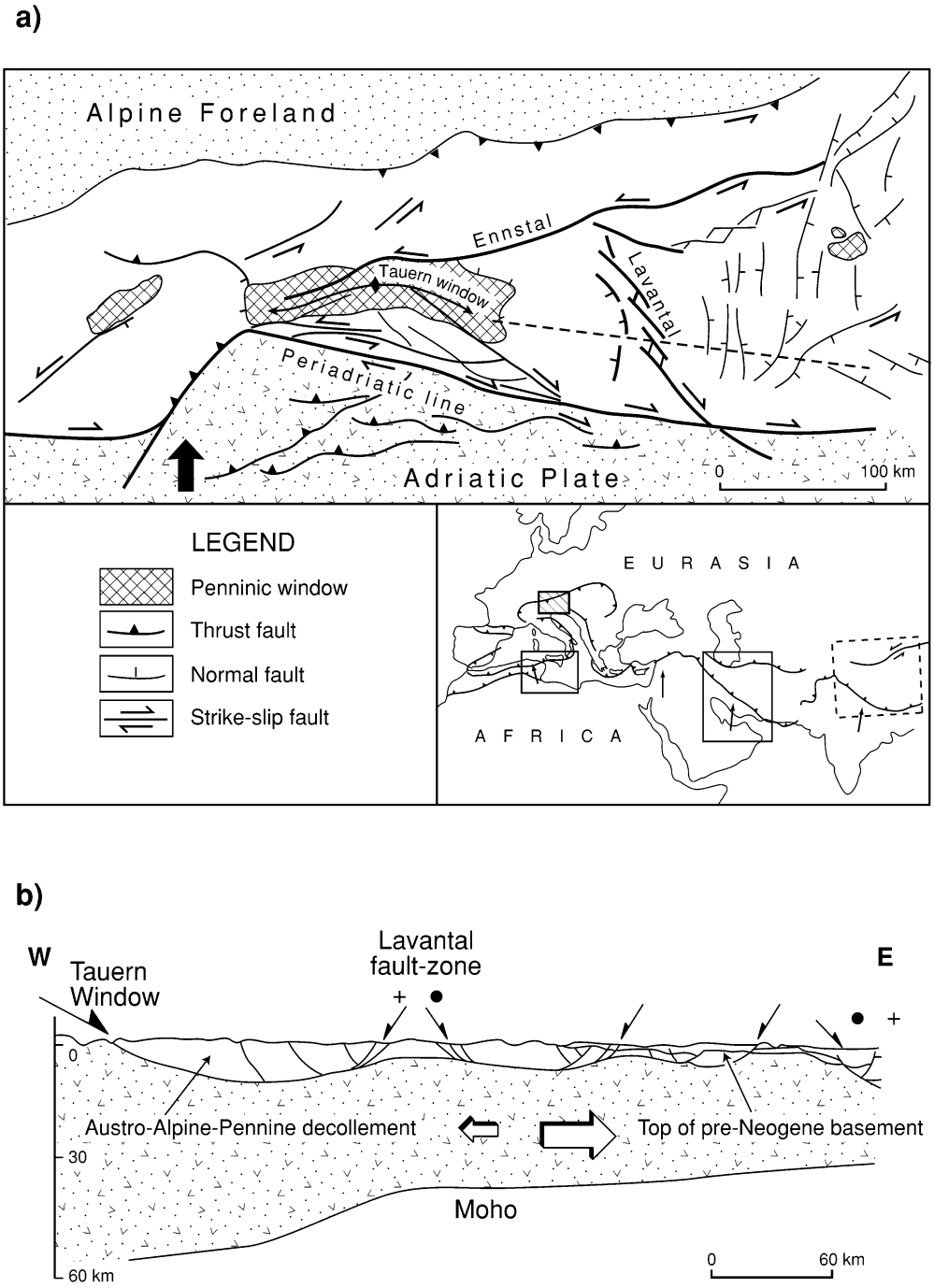

Fig. 10. Tectonic sketch map (a) of Eastern Alps; the trace of the approximately E–W-trending crustal cross-section (b) is indicated by dashed line on the map (after Ratschbacher et al., 1991a,b).

indenter dips at any angle other than the angle of internal friction of the indented material, part of the indented material is transferred onto the leading edge of the rigid indenter. Vertical escape thereafter occurs by the rise of a triangular orogenic wedge between spontaneous fore thrusts and/or back thrusts with dips close to 30° in the indented material. This transfer of laterally compacted material defines an effective indenter behind a face more mechanically efficient than the front of the initial rigid indenter. In essence, the 'most efficient' indenters are those with a front face dipping at the angle of internal friction of the indented material ($30 \pm 15°$). If the initial indenter does not start with this dip, accretion of indented material soon ensures that an effective indenter does develop this dip.

This model characterizes a type of effective indenter as a local cross-sectional structure with a horizontal scale close to the thickness of indented material.

A strip of indented material with the low deformation indicative of an effective indenter developed in front of rigid initial indenters in a number of previously reported analogue experiments (e.g. Faccenna et al., 1996, experiment E4; Davy and Cobbold 1991, models 2 and 3; Ratschbacher et al., 1991a,b, experiments 4 and 5). The planform of these effective indenters depended on particular lateral boundary conditions. The horizontal scales for this kind of effective indenter are larger than the thicknesses of the indented material. The effective indenter discussed in our model is of this type, and the structure developed depended on the 3D geometry of the experiment.

By contrast, there have been no indications of effective indenters developing in planforms of numerical models based on ductile versions of England and McKenzie's (1983) thin sheet approximation (e.g. Houseman and England, 1993; Sobouti and Arkani-Hamed, 1996). A more sophisticated approach by Ellis (1996) encountered indentation problems similar to that discussed here. However, as none of these numerical approaches can accommodate either folding or brittle shear (Medvedev and Podladchikov, 1999a), they are incapable of recognizing the spontaneous transfer of indented material to build a planform effective indenter onto the front the initial indenter. (However, some numerical models simulate the development of a local effective indenter during vertical escape, e.g. Braun and Beaumont, 1995.)

Several earlier analogue (Ratschbacher et al., 1991a) and numerical experiments (e.g. Houseman and England, 1993) attempting to simulate cases of natural indentation tailored their initial indenter to match what we consider to be the effective indenter in nature. This approach is generally inappropriate because accretion of indented material automatically reshapes a more mechanically efficient effective indenter. It is noticeable that these models failed to induce the gravity spreading significant in most natural examples.

7.2. Obliquity between vertical escape and suture

An important feature of our experiment is that the effective indenter includes part of the initially indented continent (above a fore thrust or below a back thrust separate from the suture along the initial indenter face). This means that, soon after ocean closure, the effective plate boundary might be expected to migrate from the suture decorated by slivers of ophiolite to a spontaneous intracontinental fore- or back-thrust well within the indented continent.

Our experiment thus indicates that the effective plate boundary need not parallel the main suture which closed the ocean. However, this feature is conspicuous by its absence from all the natural examples we quote. Thus, the relevant sutures parallel the zones of vertical escape and occur in different locations across them, in the Zagros, the Tell chain, the Eastern Alps and the Himalaya. In all these natural examples, not only is the zone of vertical escape structures oblique to the convergence direction but so also is the initial suture.

Vertical escape structures propagated to different degrees into each of the indenting continent. Thus, nearly all the vertical escape in the Zagros was southward over indenting Arabia, while in Palagia, most was northward over indenting Europe, and decreasing proportions occurred in the continents indenting the Himalaya and the Eastern Alps. These proportions presumably

reflect the relative strengths of the indented and indenting continents.

There must, therefore, have been another factor in these natural cases not explored in our experiment. This is likely to be that the initial sutures themselves were oblique to the convergence direction.

Extrapolating from profiles to plan forms, the concept that accretion builds an effective indenter implies that initial indenters closing along sutures oblique to the convergence direction might develop spontaneous effective front faces oblique to the suture and even more oblique to the convergence direction. All of the natural examples appear to be examples of sutures oblique to the convergence direction. Why, then, did vertical escape structures in these situations accrete an effective indenter parallel to the initial indenter?

The most obvious explanation is that, because continents are thin sheets with vertical sections weaker than lateral sections, vertical escape occurs along proximal thrusts long before horizontal escape occurs along distal strike-slip shears. The geometry of the initial indenter therefore controls the geometry of early vertical escape rather than the geometry of later lateral escape. Where continental sutures start oblique to the convergence direction, the effective indenter develops to increase the efficiency of vertical escape rather than horizontal escape. We therefore neglect this significant difference between the natural cases and our experiment and refocus on the obliquity of vertical escape.

7.3. Qualitative comparison between experiment and natural examples

Geologists and geophysicists usually construct crustal profiles across orogens; here, we emphasize the dynamic significance of changes in crustal thickness that are visible only in profiles along the orogen. The above sections have described several natural examples where the indented continent changed thickness across the direction of post-suturing convergence. Although the crustal configurations are not identical, they share many key characteristics both with each other and with our experiment. The lateral change in thickness of the indented 'continent' in the experiment induced vertical escape in an 'orogen' oblique to the convergence direction. A triangular domain of thick 'continental crust' laterally escaped toward thinner 'continental crust' between confined lateral boundaries.

The Iranian plateau–Lut block system bears the closest comparison with our experiment because the equivalent lateral boundaries appear to have been sufficiently well constrained for the fault pattern in Iran to be remarkably similar to that in the model (Fig. 11A–A′). The extrusion of the thicker block (block A and Iranian plateau) towards the thinner block (block B and Lut block) is recognizable in both natural and experimental settings. Dextral displacement associated with top-to-the left-directed thrusting along belt IA in the model is matched by similar displacements in the Zagros. Similarly, contemporaneous thrusting and sinistral transpression that occurred along belt IIA in the model occurred along the Great Kavir fault in Iran (Fig. 11A′). Moreover, the shortening structures just east of the Δ belt in the experiment and the E–W shortening of salt diapirs along the Tabas–Kerman lineament in Iran can both be attributed to eastward escape and gravity spreading of a thick Central Iran toward the thinner Lut block between conjugate strike-slip fault zones opening eastward (Fig. 11A′). Finally, the Makran belt, the Elburz–Kopet Dagh and the complex pattern of folds produced at high angles to the eastern boundary of the Lut block all match equivalent structures in the experiment (Fig. 11A–A′).

An obvious difference between the Iranian plateau–Lut block system and our model is that the Great Kavir fault does not appear to have developed to the same maturity as the corresponding belt IIA in our model. A more obvious difference is that the suture zone in this natural example is behind the Zagros fold-thrust belt (Fig. 11A′) rather than perpendicular to the convergence direction and along the southern boundary of Fig. 11A′ as simulated in the model. We therefore infer that the suture along which the Zagros closed began oblique to the convergence direction and that, rather than a weak triangular domain of Asia transferring across the plate boundary, vertical

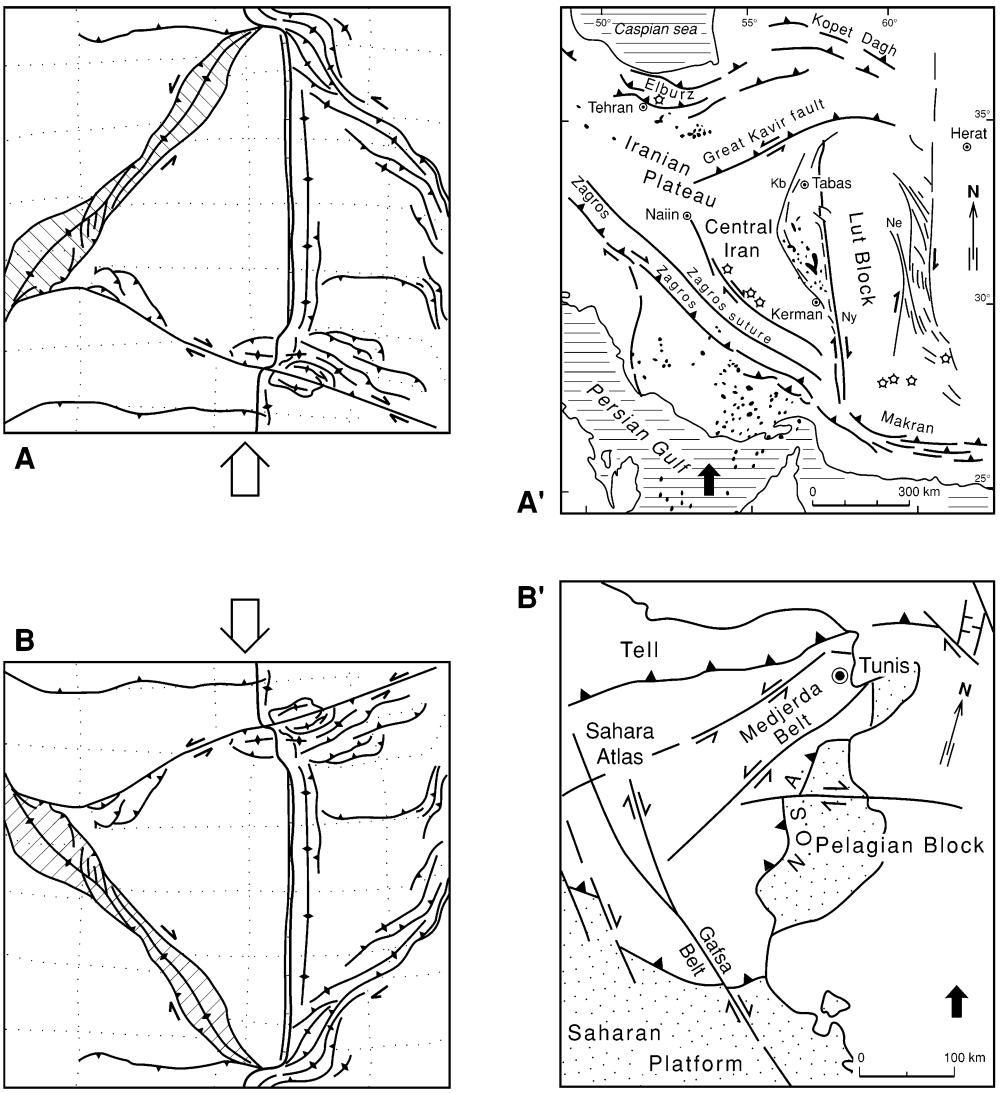

Fig. 11. Comparison between the model and natural examples: A–A′) Zagros–Iranian plateau and Lut block (after Fig. 8), B–B′) Tell–Atlas and Pelagian block (after Fig. 9). To aid comparison, map B has been inverted and map B′ slightly rotated.

escape involves the weaker Phanerozoic sediments topping the Arabian plate. Pre-suturing accretion (visible in the Makran) and post-suturing accretion (in the Zagros) maintained the same polarity, probably because the Phanerozoic carbonate cover in the SE Zagros overlies the Hormuz salt (Talbot and Alavi, 1996).

The main structural features in and around the Tell–Atlas–Pelagian block system match those in the model if the experiment is inverted (Fig. 11B) so that our experimental configuration conforms with the geography (Fig. 11B′). Thus, the Gafsa and Medjeda strike-slip belts match belts IA and IIA in the model (cf. Fig. 11B and B′) and the east-verging thrust-fold belt developed along the NOSA belt (Anderson, 1996) is comparable with the welt developed alongside the Δ belt in the experiment. Comparison with our experiment suggests that the Pelagian block remained comparatively unaffected while the crust in the Tell–Atlas

sector thickened during Alpine orogenesis. Here, too, the suture (obscure in the Tell chain) is parallel to the vertical escape structures and therefore closed already oblique to the convergence direction.

Lateral escape of the Eastern Alps was eastward and toward a subduction zone around the Pannonian arc well beyond the front of the indenter (Ratschbacher et al., 1991a,b). In this sense, the Eastern Alps are closer to previous models than ours in which the lateral constraint was in front of the indenter. However, although the Eastern Alps are noticeably oblique to the convergence direction, so is the suture which is along the Periadiatic line and parallel to the eastern Alps.

Two factors point to the Alpine sector having developed further than the stage at which we ceased shortening our experiment. The main conjugate strike-slip shear zones between which Eastern Alpine crust escaped eastward, the Ennstal and Periadriatic lines, are equivalent to belts IIA and belt IA in the model and display sinistral and dextral transpression respectively. The angle between belts IA and IIA decreased during bulk shortening in the experiment (Fig. 4), so the angle between the Periadriatic and Ennstal lines, (Fig. 10a), which is smaller than equivalent angles in Iran (Fig. 8) and Tunisia (Fig. 9), may indicate a higher bulk shortening across the Swiss Alps (see also Kurz et al., 1996; Lammerer and Weger, 1998) than in the other examples (and the experiment). As in Iran, the Periadriatic suture in the Eastern Alps appears to have been oblique to the direction of convergence when it closed. As a result, the initial suture may have continued to act as the face of the effective Adriatic indenter and some of the vertical escape propagated southward into the indenter.

Our experiment also bares comparison with the Himalaya–Tibet system (figs. 4 and 5 in Cobbold and Davy, 1988). Taking India as the initial indenter, the Himalaya mountains as belt system I, and the Tarim basin as domain AIII, the Tien Shan and Altai transpressive faults systems could match the no-slip distal boundary of our experiment. Because the weak lateral boundary is far to the east of Tibet, we compare the present state of the indentation of Asia by India with the second stage of deformation in our model. This was characterized by the development of strike slip belts IIA (equivalent to the Altyn–Tagh fault along the northern border of Tibet) and thrust system IIB (the north-east margin of the Tibetan plateau) along which most of the north-eastward motion of the Tibetan plateau occurred (Cobbold and Davy, 1988). The EW gravity collapse of the Tibetan plateau (Dewey, 1988) compares well with the EW extension seen across domain AII in the experiment. Here, too, the initial sutures appear to have been oblique to the convergence direction, and vertical escape appears to have occurred oblique to the convergence direction and on both sides of the initial suture.

7.4. Quantitative comparison between experiment and natural examples

A quantitative comparison between our experiment and natural examples allows us to rationalize the difference between only vertical escape structures being oblique to the convergence direction in our model and both vertical escape structures and sutures being oblique to the convergence direction in nature.

Repeated scaling analyses and dynamically scaled analogue experiments (Davy and Cobbold, 1991) show that continental lithosphere folds wherever it has been shortened significantly, usually on wavelengths longer than 100 km (Stephenson and Cloetingh, 1991), as is particularly obvious near the Alpine–Himalayan orogen (Burov et al., 1993).

We have already attributed the spontaneous obliquity between the vertical escape structures and the convergence direction in our model to the mutual interference between the wavelengths of early vertical escape structures relating to the different strengths or thicknesses of the indented blocks A and B. We argue that the same argument applies to the obliquity between the vertical escape structures and the convergence direction in our chosen natural examples.

As a measure of obliquity in both experiment and nature, we use Δ_λ, the distance between the ends of the oblique sector projected onto the

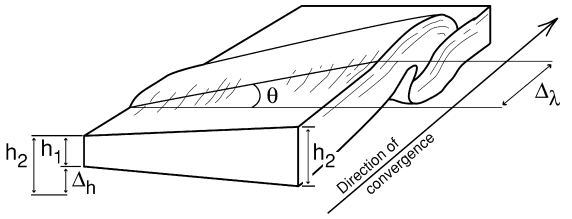

Fig. 12. Obliquity parameters used in the quantitative analyses.

convergence direction (Fig. 12). Thus, Δ_λ equals zero for orogenic belts perpendicular to the convergence direction. The conclusions of our dynamic interpretations of the experiment show that finite Δ_λ for orogens oblique to the convergence direction depends on lateral variations in thickness, Δ_h, of the upper crust (Fig. 12). Δ_h, was equal to 0.3 cm in the experiment (Fig. 2). In natural examples, Δ_h can be approximated by half the lateral variations in total thickness of the crust, and the 'obliquity ratio' Δ_λ/Δ_h allows a quantitative comparison between the experiment and natural examples (Table 2) and discussion.

The obliquity ratio of the experiment compares well with what we know of the crustal configuration in and around Tunisia (Fig. 9), where the Tell thrust is assumed to have been the initial indenter and the Madjerda Belt as bounding the effective indenter.

The obliquity ratio in Iran is high compared to our experiment (Table 1). Two additional factors could raise the obliquity ratio in Iran. First, lateral differences in strength are exaggerated by salt within the upper crust, which significantly weakens the eastern Zagros (Talbot and Alavi, 1996) and the central Lut block. Second, the rotation of Arabia could have changed the convergence direction. Collisions that began more SW–NE than the current S–N convergence direction would decrease the obliquity ratio.

We attribute the low obliquity ratio for the Eastern Alps (Table 2) to the greater degree of convergence than that reached in our experiment. The comparison would have been closer if our model had been shortened further.

The very high obliquity ratio for the Himalaya–Tibet system (Table 1) is subject to assumptions about the thickness of the crust. Our model did not take account of any influence of a stiff upper mantle despite previous analyses assuming that the upper mantle is coupled with the crust in Himalaya–Tibet system (e.g. Burov et al., 1993). The addition of a stiff upper mantle to our experiment would increase its obliquity ratio.

There is a crude but direct relationship between the obliquity angle, θ (Table 2), and where vertical escape occurred relative to the initial suture in our natural examples. Different proportions of the vertical escape structures propagated from the indented continents into the indenting continent.

The highest obliquity angle ($\theta \approx 35^\circ$) is in Iran where nearly all the vertical escape occurred in indenting Arabia rather than indented Asia. Palagia and the Himalaya share an intermediate obliquity angle ($\theta \approx 25^\circ$), and low but significant proportions of vertical escape involved the leading edges of indenting Europe and India, respectively. The lowest obliquity angle ($\theta \approx 15^\circ$) is in the Eastern Alps where very little vertical escape occurred in indenting Adria, and the vast majority occurred in indented Europe. We interpret these proportions as reflecting the relative strengths of the indented and indenting continents.

Rates of lateral escape also support the model

Table 2
Parameters of obliquity in the experiment and natural examples

	Experiment	Zagros	Tunisia	Alps	Tibet
Obliquity angle, θ	20°	35°	25°	15°	25°
Δ_λ	7 cm	300 km	120 km	50 km	600 km
Δ_h	0.3 cm	10 km	5 km	6 km	10 km (?)
Obliquity angle, Δ_λ/Δ_h	23	30	24	8	60 (?)

presented here. Isostatic adjustment of the initial configuration in our experiment was active throughout but, even in its final stages, appears to have influenced its general pattern of deformation very little. The estimated ratio of the initial rate of isostatic adjustment to the convergence rate was about 7% in the experiment [Appendix A, Eq. (8)]. Nevertheless, this allows comparison between the results of numerical experiments with field observations. Numerical experiments that neglect possible initial lateral variations in thickness calculate rates of lateral escape less than 20% of the convergence rate in the Himalaya–Tibet system (Houseman and England, 1993), much lower than the 25% suggested by field observations (Molnar and Deng, 1984).

8. Summary and conclusions

Previous studies of indentation tectonics focused mainly on the lateral escape of laterally uniform indented material toward weak lateral boundaries far beyond the indenter. This study focused on vertical escape in a continent with a built-in thickness change confined by lateral boundaries in front of the indender. Vertical escape was already known to occur in a thrust-bound wedge in front of an effective indenter accreted onto the initial indenter with geometries that depend on the angle of internal friction and the thickness of the indented material.

Vertical escape in our experiment began with different structural wavelengths in two indented blocks with different thickness. As these two sets of vertical escape structures propagated toward each other, they interacted and straightened as they merged into a single model orogen oblique to both the convergence direction and the model suture.

By contrast, the natural orogenic belts and sutures that we considered parallel each other, so both are oblique to the convergence direction. An additional difference is that all the vertical escape in the experimental sand pack occured in front of an indenter that was rigid, whereas vertical escape structures propagated into both the indented and indenting continents. Adding the lessons of the natural examples to those of our experiment, the initial indenter can act as the effective indenter in map view if it closes oblique to the convergence direction. Vertical escape structures develop parallel to an initial suture that is oblique to the convergence direction and can involve both converging continents in a ratio that probably depends on their relative strengths and the orientations of their margins.

We conclude that:

(1) Lateral variation in strength or thickness of the indented material along a direction perpendicular to its convergence direction introduces an obliquity to early vertical escape structures in map view that influences subsequent lateral escape structures.

(2) Comparison to nature (Alps–Himalayas) shows that lateral steps or gradients of an indented continent lead to oblique structures irrespective of the suture orientation.

(3) Gravity spreading along transpressive zones aids escape.

(4) Experiments support the reversal of the pre- and post-suturing polarity of accretion. Natural examples show that the direction of accretion depends on the strength and orientation of sutured continental margins.

(5) Extended thin sheet approximation helps analogue experiments by:

- distinguishing deformation features;
- estimating how rates of vertical and lateral orogenic escape and gravity spreading relate to the driving forces.

Acknowledgements

We acknowledge research grants by the Swedish National Research Council (NFR), Uppsala University and the Italian National Research Council (CNR) 'Centro di Studio di Geologia dell'Appennino e delle Catene Perimediterranee' of Firenze (Publ. no. 315). Prof. J.-P. Burg, Y.Y. Podladchikov, G. Mulugeta and K. Persson are thanked for valuable discussions. We are particularly greatful to the three reviewers E. Burov, A. Henk and an anonymous reviewer for their constructive criticisms. C. Wernström is thanked for drafting the figures.

Appendix A: Rates of isostatic adjustment and gravity spreading

While the external forces (e.g. the pushing of the moving wall) are known parameters of the model, the deformations due to internal forces cannot be clearly defined by measurements and observations. We estimate these forces and deformations by analysis. The aim is not to obtain a complete numerical integration of the system but to define the order of influence of gravity. Therefore, we perform rough estimates using the following simplifications:

(1) The sand layer exerts only a normal load on the underlying viscous layers. This great simplification would not affect the results significantly if the rates of considered deformations are small, so that deformations due to gravity are concentrated in the viscous layers.

(2) Flexural rigidities of the competent layers are neglected. This assumption is acceptable for directions perpendicular to the external applied forces but may lead to oversimplification in actively deforming structures.

The parameter, ϵ, presented in Table 1 is very small for all cases, and this allows us to apply thin sheet approximations. The advantages and disadvantages of a number of thin sheet approximations currently used in geodynamics are described by Medvedev and Podladchikov (1999a). We found that only the Extended Thin Sheet Approximation (ETSA) is able to describe both isostatic adjustment and gravity spreading.

The leading asymptotic terms in the horizontal velocity field can be estimated using ETSA for 2D cases as follows (Medvedev and Podladchikov, 1999b):

$$V_x(x,z)=R_s\int_0^z\frac{dz'}{\mu}-\frac{\partial R_n}{\partial x}\int_0^z\frac{z'dz'}{\mu}-\int_0^z\left[\frac{1}{\mu}\int_0^{z''}\frac{\partial}{\partial x}\left(\int_0^{z''}\rho g\,dz'''\right)dz''\right]dz'. \quad (1)$$

Here, $V_x(x,z)$ is the horizontal velocity, R_s is the shear stress, R_n is the normal stress along the bottom boundary ($z=0$), μ is the viscosity, ρ is the density and g is the acceleration due to gravity. The rheological parameters (m and r) change from the asthenosphere (m_a and r_a) up to the ductile crust (μ_d and ρ_d) in integrals of Eq. (1). The coordinate system (x, z) is shown on Fig. 3.

Basal stresses can be approximated by using vertical and horizontal balances of force averaged over depth (from the base, $z=0$, up to the topographic surface, $z=S$). After applying the horizontal boundary conditions to the experimental settings, ETSA gives the asymptotic approximation of balance of forces in the form:

$$R_n=-\int_0^S\rho g\,dz' \quad (2)$$

$$-R_s+\frac{\partial}{\partial x}(R_nH+\bar{\rho}g)+4\epsilon^2h_d\frac{\mu_d}{\mu_a}\frac{\partial^2}{\partial x^2}\left(h_a\left(R_{sI}-\frac{h_a}{2}\frac{\partial R_n}{\partial x}\right)\right)=0 \quad (3)$$

where H ($=h_a+h_d+h_u$) is the total thickness of the experimental lithosphere. Thicknesses of rheological layers are denoted by h with indices: 'a' for the asthenosphere (syrup), 'd' for the ductile crust (silicone mixture) and 'u' for the upper brittle part of the crust (sand). The double integrated density throughout the lithosphere is denoted as $\bar{\rho}$.

Eqs. (1)–(3) operate with dimensionless parameters. Following Medvedev and Podladchikov (1999a), we adopted two geometrical length scales (horizontal, L, and vertical, H), and then dimensionless coordinates can be expressed via dimensional coordinates, denoted by superscript 'd', as in $x=x^d/L$, $z=z^d/H$. This emphasizes the geometrical singularity of the model. The small parameter, ϵ, in Eq. (3) is the result of such scaling. The natural dimensional scale for the basal stresses is (ρgH) and for velocity is ($\epsilon\rho gH^2/\mu$). The choice of scales for other parameters does not play any significance in the following developments.

The high orders of asymptotic treatment by ETSA emphasize the importance of high-order derivative terms in the balance of forces when describing deformations in systems which can have very uneven rheological stratification. Previous analytical approximations ignored the third terms

describing the force balance [Eq. (3)] because of geometrical singularity ($\epsilon \ll 1$). However, this term is the most important in systems with high competence contrast between layers because of factor $\mu_d/\mu_a \sim 10^5$ ($\gg 1$ and even $\gg \epsilon^{-2}$).

Eqs. (1)–(3) allow us to estimate velocity profiles during different stages of isostatic adjustment. For the first stage (when $R_n = \text{const}$) Eq. (3) gives:

$$\frac{\partial^2}{\partial x^2}\left(h_a\left(R_{sI} - \frac{h_a}{2}\frac{\partial R_n}{\partial x}\right)\right) \approx 0 \tag{4}$$

which can be resolved as:

$$R_{sI} \approx \frac{h_a}{2}\frac{\partial R_n}{\partial x}. \tag{5}$$

Substitution of Eq. (5) into Eq. (1) allows the conclusion that the ratio of characteristic horizontal velocities in the mantle and ductile crust is large and is expressed as $V_{aI}/V_{dI} \sim \mu_a/\mu_d$ during the first stage of isostatic adjustment. This ratio indicates a horizontal channel flow in the asthenosphere. The most significant motions in the ductile crust are vertical. The mass conservation constraint gives:

$$W_{dI} = -\epsilon \int_0^z \frac{\partial V_x}{\partial x}\,dz' \approx -\frac{\rho_u g h_a^3}{12\mu_a}\frac{\Delta_h}{L^2} \sim 10^{-4}\ \text{m/s (0.1 mm/s)}. \tag{6}$$

This approach allows us to conclude that the second stage of isostatic adjustment (Airy isostasy) takes several minutes in the model. This stage is characterized by the condition of no variations of normal stress along the base of the model, $R_n = \text{const}$. The second and third terms in Eq. (3) became more important during the second stage of isostatic adjustment and give:

$$R_{sII} \approx \frac{\Delta_\rho \phi g \Delta_h L}{4h_a}\frac{\mu_a}{\mu_d} \tag{7}$$

where $\Delta_r = \rho_u - \rho_a$ is the difference in density between sand and syrup and $\phi = (1 - \rho_u/\rho_a)$ is the isostatic amplification factor. Substitution of Eq. (7) into Eq. (1) estimates the horizontal velocity in the lower crust during the second stage:

$$V_{dII}(x) \approx \frac{\Delta_\rho \phi g \Delta_h L}{4\mu_d} \sim 3 \times 10^{-7}\ \text{m/s (0.1 cm/h)} \tag{8}$$

Eq. (8) allows the conclusion that deformations due to the second stage of isostatic adjustment are significant throughout the experiment.

Estimates in this section were compared to the results of experiments on isostatic adjustment by Ramberg (1968). The simplifications in our model play a significant role in the first stage and give adjustment rates 4–6 times greater than those in Ramberg's experiment. Estimates regarding the second stage are in good agreement with Ramberg with an error of less than 50%. Unlike other approximations, ETSA allowed us to estimate these rates throughout the development of the adjustment. Adopting the terminology of Medvedev and Podladchikov (1999a), the 'SS' approach (e.g. Medvedev, 1993) gives rates about two orders higher than Ramberg (1968), while th 'PS' approach (England and McKenzie, 1983) cannot be applied to the first stage of isostatic adjustment.

The above estimates were for the initial stages of our experiment. However, these results can be extended to the later stages of deformations when the system developed by continuous shortening. We can conclude that during progressive deformations: (1) the system indicates local (Airy) isostasy and (2) the rate of gravity spreading in the crust can be roughly estimated by Eq. (8) after substitution of the actual difference in thickness of the sand layer, Δ_h.

References

Alavi, M., 1992. Thrust tectonics in the Bidalood region: NE Iran. Tectonics 11, 360–370.

Anderson, J.E., 1996. The Neogene structural evolution of the western margin of the Pelagian Platform, central Tunisia. J. Struct. Geol. 18, 819–833.

Argand, E., 1924. La tectonique de l'Asie. Compte Rendu de la 13ème Congres Géologique International, Brussels Vol. 1., 171–372.

Artyushkov, E.V., 1974. Can the Earth's Crust be in a state of isostasy? J. Geophys. Res. 79, 741–752.

Backofen, W.A., 1972. Deformation Processing. Addison Wesley, Reading, MA.

Balla, Z., 1985. The Carpathian loop and the Pannonian basin: a kinematic analysis. Geophys. Trans. 30, 313–353.

Biju-Duval, B.J., Dercourt, J., Le Pichon, X., 1977. From the Tethys Ocean to the Mediterranean sea: a plate tectonic model for the evolution of western Alpine system. In: Biju-Duval, B.J., Montandert, L. (Eds.), Structural History of the Mediterranean Basin. XXV Congrès CIESM Vol. X. Technip, Paris, pp. 143–164.

Boccaletti, M., Dainelli, P., 1982. Il sistema neogenico-quaternario nell'area mediterranea: esempio di deformazione plastico-rigida post-collisionale. Mem. Soc. Geol. It. 24, 465–482.

Boccaletti, M., Conedera, C., Dainelli, P., Gocev, P., 1982. The Recent (Miocene–Quaternary) Regmatic System of the Western Mediterranean region. J. Petrol. Geol. 5, 31–49.

Boccaletti, M., Nicolich, R., Tortorici, L., 1984. The Calabrian arc and the Ionian sea in the dynamic evolution of the Central Mediterranean. Mar. Geol. 55, 219–245.

Boccaletti, M., Conedera, C., Dainelli, P., Gocev, P., 1985. Tectonics Map of the Western Mediterranean Area, Scale 1:2,500,000. Litografia Artistica Cartografica, Florence.

Boccaletti, M., Cello, G., Tortorici, L., 1987. Neogene–Quaternary tectonics of central Tunisia: implications for a full-scale model of the Western Mediterranean. Acta Naturalia de l'Ateneo Parmense 23, 201–210.

Boccaletti, M., Cello, G., Tortorici, L., 1988. Structure and tectonic significance of the north–south axis of Tunisia. Annales Tectonicae 2, 12–20.

Boccaletti, M., Cello, G., Tortorici, L., 1990. First order kinematic elements in Tunisia and the Pelagian block. Tectonophysics 176, 215–228.

Bonini, M., Sokoutis, D., Talbot, C.J., Bocaletti, M., Milnes, A.G., 1999. Indenter growth in analogue models of Alpine-type deformation. Tectonics 18, 119–128.

Braun, J., Beaumont, C., 1995. Three dimensional numerical experiments of strain partitioning at oblique plate boundaries: Implications for contrasting tectonic styles in the southern Coast Ranges, California and central South Island, New Zealand. J. Geophys. Res. 100, 18059–18074.

Buck, R.W., 1997. Bending thin lithosphere causes localized 'snapping' and not distributed 'crunching': Implications for abyssal hill formation. Geophys. Res. Lett. 24, 2531–2534.

Burchfiel, B.C., Royden, L., 1982. Carpathian foreland fold and thrust belt and its relation to Pannonian and other basins. Am. Assoc. Petrol. Geol. Bull. 66, 1179–1195.

Burke, K., Sengör, M.C., 1986. Tectonic escape in the evolution of continental crust. In: Barazangi, M., Brown, L. (Eds.), Reflection Seismology: The Continental Crust, Geodyn Ser. Vol. 14. AGU, Washington, DC, pp. 41–53.

Burov, E.B., Lobkovsky, L.I., Cloetingh, S., Nikishin, A.M., 1993. Continental lithosphere folding in Central Asia (part 2), constraints from gravity and topography. Tectonophysics 226, 73–87.

Burov, E.B., Diament, M., 1995. The effective elastic thickness (T_e) of continental lithosphere: What does it really mean? J. Geophys. Res. 100, 3905–3927.

Carey, S.W., 1958. The tectonic approach to continental drift. Continental Drift Symposium, Univ. Tasmania, 177–355.

Carter, N.L., Tsenn, N.C., 1987. Flow properties of continental lithosphere. Tectonophysics 136, 27–64.

Cassinis, R., 1983. Seismicity and crustal structure in the Italian Region: preliminary zoning. Boll. Geof. Teor. Appl. 97, 3–26.

Chase, C.G., 1978. Plate kinematics: the Americas, East Africa and the rest of the world. Earth Planet. Sci. Lett. 37, 357–368.

Cloetingh, S., Burov, B., 1996. Thermomechanical structure of European continental lithosphere constrain from rheological profiles and EET estimates. Geophys. J. Int. 124, 695–723.

Cobbold, P.R., Davy, P., 1988. Indentation tectonics in nature and experiments, 2, Central Asia. Bull. Geol. Inst. Univ. Uppsala 14, 143–162.

Cobbold, P.R., Szatmari, P., Demercian, L.S., Coelho, D., Rossello, E.A., 1995. Seismic and experimental evidence for thin-skinned horizontal shortening by convergent radial glidding on evaporites, deep-water Santos Basin, Brazil. In: Jackson, M.P.A., Roberts, D.G., Snelson, S. (Eds.), Salt Tectonics: A Global Perspective. AAPG Memoir Vol. 65., 305–321.

Cohen, C.R., Schamel, S., Boyd-Kaygi, P., 1980. Neogene deformation in northern Tunisia: the origin of the eastern Atlas by microplate-continental margin collision. Bull. Geol. Soc. Am. 91, 225–237.

Davis, D., Suppe, J., Dahlen, F.A., 1983. Mechanics of fold and thrustbelts and accretionary wedges. J. Geophys. Res. 88, 1153–1172.

Davy, P., Cobbold, P.R., 1988. Indentation Tectonics in Nature and Experiments, 1. Experiments scaled for gravity. Bull. Geol. Inst. Univ. Uppsala 14, 129–141.

Davy, P., Cobbold, P.R., 1991. Experiments on shortening of a 4-layer continental Lithosphere. Tectonophysics 188, 1–25.

Dehghani, G.A., Makris, J., 1983. The gravity field and custal structure of Iran. Geodynamics Project (Geotraverse) in Iran, Geological Survey of Iran, Rep. No. 51, 51–68.

DeMets, C., Gordon, R.G., Argus, D.F., Stein, S., 1990. Current plate motions. Geophys. J. Int. 101, 425–478.

Dewey, J.F., Pitman, W.C., Ryan, W.B.F., Bonnin, J., 1973. Plate tectonics and the evolution of the Alpine system. Bull. Soc. Geol. Am. 84, 3138–3180.

Dewey, J.F., 1988. Extensional collapse of orogens. Tectonics 7, 1123–1139.

Dewey, J.F., Helman, M.L., Turco, E., Hutton, D.H.W., Knott, S.D., 1989. Kinematics of the Western Mediterranean. In: Coward, M.P., Dietrich, D., Park, R.G. (Eds.), Alpine Tectonics. Geol. Soc. Spec. Publ. 45, 265–283.

Ellis, S., 1996. Forces driving continental collision: Reconciling indentation and mantle subduction tectonics. Geology 24, 699–702.

England, P., McKenzie, D., 1983. Correction to: a thin viscous sheet model for continental deformation. Geophys. J. R. Astron. Soc. 73, 523–532.

Faccenna, C., Davy, P., Brun, J.P., Funiciello, R., Giardini, D., Mattei, M., Nalpas, T., 1996. The dynamics of back-arc extension: an experimental approach to the opening of the Tyrrhenian Sea. Geophys. J. Int. 126, 781–795.

Genser, J.van, Wees, J.D., Cloethingh, S., 1996. Eastern Alpine tectono-metamorphic evolution, constraints from two-dimensional *P–T–t* modeling. Tectonics 15, 584–604.

Gerbault, M., Poliakov, A.N.B., Diagnieres, M., 1998. Prediction of faulting from the theories of elasticity and plasticity: what are the limits? J. Struct. Geol. 20, 301–320.

Giese, P., Reutter, K.J., Jacopshagen, V., Nicolich, R., 1982. Explosion seismic crustal studies in the Alpine Mediterranean region and their implications to tectonic processes. In: Berckhemer, H., Hsü, K.J. (Eds.), Alpine Mediterranean Geodynamics. Geodyn. Ser. Vol. 7. AGU, Washinghton, DC, pp. 39–73.

Giese, P., Makris, G., Akashe, B., Power, P., Letz, H., Mostaanpour, M., 1983. Seismic crustal studied in southern Iran between the Central Iran and the Zagros belt. Geodynamics Project (Geotraverse) in Iran, Geological Survey of Iran, Rep. No. 51, 71–89.

Hearn, T.M., Ni, J.F., 1994. Pn velocities beneath continental collision zones: the Turkish–Iranian Plateau. Geophys. J. Int. 117, 273–283.

Hlaiem, A., Biju-Duval, B., Vially, R., Laatar, E., M'Rabet, A., 1997. Burial and thermal history modelling of the Gafsa–Metlaoui intracontinental basin (Southern Tunisia): implications for petroleum exploration. J. Petrol. Geology 20, 403–426.

Houseman, G., England, P., 1993. Crustal thickening versus lateral expulsion in the Indian–Asian continental collision. J. Geophys. Res. 98, 12233–12249.

Jackson, J., Fitch, T., 1981. Basement faulting and the focal depths of the larger earthquakes in the Zagros mountains (Iran). Geophys. J. R. Astron. Soc. 64, 561–586.

Jackson, J.A., McKenzie, D., 1984. Active tectonics of the Alpine–Himalayan belt between western Turkey and Pakistan. Geophys. J. R. Astron. Soc. 77, 185–264.

Jackson, J.A., McKenzie, D., 1988. The relationship between plate motions and seismic moment tensors, and the rates of active deformation in the Mediterranean and the Middle East. Geophys. J. R. Astron. Soc. 93, 45–73.

Jackson, M.P.A., Cornelius, R.R., Craig, C.H., Gansser, A., Stöcklin, J., Talbot, C.J., 1990. Salt diapirs of the Great Kavir, Central Iran. Geol. Soc. Am., Mem. 177, 139 pp.

Kirby, R.H., 1983. Rheology of the lithosphere. Rev. Geophys. Space Phys. 21, 1458–1487.

Kirby, R.H., 1985. Rock mechanic observations pertinent to the rheology of the continental lithosphere and the localization of strain along shear zones. Tectonophysics 119, 1–27.

Kurz, W., Neubauer, F., Genser, J., 1996. Kinematics of Penninic nappes (Glockner Nappe and basement-cover nappes) in the Tauern Window (Eastern Alps, Austria) during subduction and Penninic–Austroalpine collision. Eclogae Geol. Helv. 89 (1), 573–605.

Lammerer, B., Weger, M., 1998. Footwall uplift in an orogenic wedge: the Tauern Window in the Eastern Alps of Europe. Tectonophysics 285, 213–230.

Le Pichon, X., 1968. Sea-floor spreading and continental drift. J. Geophys. Res. 73, 3661–3697.

McKenzie, D.P., Parker, R.L., 1967. The North Pacific: an example of tectonics on a sphere. Nature 216, 1276–1280.

Malinverno, A., Ryan, W.B. F., 1986. Extension in the Tyrrhenian and shortening in the Apennines as results of arc migration driven by sinking of the lithosphere. Tectonics 5, 245–277.

Medvedev, S.E., 1993. Computer simulation of sedimentary cover evolution. In: Harff, J., Merriam, D.F. (Eds.), Computerized Basin Analysis: The Prognosis of Energy and Mineral Resources. Plenum Press, New York, pp. 1–10.

Medvedev, S.E., Podladchikov, Y., 1999a. New extended thin sheet approximation for geodynamic applications — I. Model formulation. Geophys. J. Int. 136, 567–585.

Medvedev, S.E., Podladchikov, Y., 1999b. New extended thin sheet approximation for geodynamic applications — II. 2D examples. Geophys. J. Int. 136, 586–608.

Mitchel, A.H.G., Garson, M.S., 1976. Mineralization at plate boundaries. Miner. Sci. Eng. 8, 129–169.

Molnar, P., Deng, Q., 1984. Faulting associated with large earthquakes and the average rate of deformation in central and eastern Asia. J. Geophys. Res. 89, 6203–6228.

Morgan, W.J., 1968. Rises, trenches, great faults and crustal blocks. J. Geophys. Res. 73, 1959–1982.

Müller, S., Ansorge, J., Egloff, R., Kissling, E., 1980. A crustal cross section along the Swiss Geotraverse from Rhinegraben to the Po Plain. Eclogae Geol. Helv. 73, 463–483.

Okaya, N., Cloethingh, S., Mueller, S., 1996. A lithospheric cross-section through the Swiss Alps — II. Constraints on the mechanical structure of a continent–continent collision zone. Geophys. J. Int. 127, 399–414.

Ouali, J., Tricart, P., Delteil, J., 1987. Ampleur et signification des recouvrements anormaux dans l'axs Nord-Sud (Tunisie centrale: donnes nouvelles dans le chainon Nara–Sidi Khalif). Eclog. Geol. Helv. 80, 685–696.

Peltzer, G., 1988. Centrifuged experiments of continental scale tectonic in Asia. Bull. Geol. Inst. Univ. Uppsala 14, 115–128.

Persson, K., submitted for publication. Orogenic wedges and indenter geometry, GSA special publication.

Pfiffner, O.A., Frei, W., Valasek, P., Stuble, M., Levato, L., DuBois, L., Schmid, S.M., Smithson, S.B., 1990. Crustal shortening in the Alpine orogen: results from deep seismic reflection profiling in the Eastern Swiss Alps, Line NFP20-EAST. Tectonics 9, 1327–1355.

Philip, H., Andrieux, J., Dlala, M., Chihi, L., Ben Ayed, N., 1986. Évolution tectonique mio-plio-quaternarie du fossé de Kasserine (Tunisie centrale): implications sur l'évolution géodynamique récente de la Tunisie. Bull. Soc. Géol. Fr. 8, 559–568.

Ramberg, H., 1968. Instability of layered systems in the field of gravity 2. Phys. Earth Planet. Inter. 1, 448–474.

Ranalli, G., 1987. Rheology of the Earth. Allen and Allen, Boston, MA. 366 pp

Ranalli, G., Murphy, D.C., 1987. Rheological stratification of the lithosphere. Tectonophysics 132, 281–296.

Ratschbacher, L., Merle, O., Davy, P., Cobbold, P., 1991a. Lateral extrusion in the eastern Alps, part 1: boundary conditions and experiments scaled for gravity. Tectonics 10, 245–256.

Ratschbacher, L., Frisch, W., Linzer, H.G., Merle, O., 1991b. Lateral extrusion in the eastern Alps, part 2: structural analysis. Tectonics 10, 257–271.

Regenauer-Lieb, K., 1996. Plastic velocity vector diagrams applied to indentation and transpression in the Alps. J. Geodynam. 21, 339–353.

Regenauer-Lieb, K., Petit, J.P., 1997. Cutting of the European continental lithosphere: Plasticity theory applied to the present Alpine collision. J. Geophys. Res. 102, 7731–7746.

Robbins, J.W., Dunn, M.H., Torrence, M.H., Williamson, R.G., Klosko, S.M., Smith, D.E., Kolenkiewicz, R., Nerem, N.S., Pavlis, E.C., 1992. SLR determined tectonic motion in the Aegean and Eastern Mediterranean. Second Working Group Meeting of the Dynamic of the Solid Earth Proc., Greenbelt, 13–15.

Rouvier, H., 1977. Géologie de l'extreme Nord tunisien: tectoniques et Paléogéographies superposées à l'extrémité or oriental e de la chaine Nord Maghrebine. Thèse Doct. d'Etat, Univ. Pierre et Marie Curie, Paris VI, 428 pp.

Royden, L., Horváth, F., Rumpler, J., 1983. Evolution of the Pannonian Basin system, 1, Tectonics. Tectonics 2, 63–90.

Royden, L., 1996. Coupling and decoupling of crust and mantle in convergent orogens: Implications for strain partitioning in the crust. J. Geophys. Res. 101, 17679–17705.

Schmid, S.M., Aebli, H.R., Heller, F., Zingg, A., 1989. The role of the Periadriatic Line in the tectonic evolution of the Alps. In: Coward, M.P., Dietrich, D., Park, R.G. (Eds.), Alpine Tectonics. Spec. Publ. Geol. Soc. Lond. 45, 153–171.

Schmid, S.M., Pfiffner, O.A., Froitzheim, N., Schunborn, G., Kissling, E., 1996. Geophysical–geological transect and tectonic evolution of the Swiss–Italian Alps. Tectonics 15, 1036–1064.

Snocke, A.W., Schamel, S., Karasek, R.M., 1988. Structural evolution of Djebel Debadib anticline: a clue to the regional tectonic style of the Tunisian Atlas. Tectonics 7, 497–516.

Snyder, D.B., Barazangi, M., 1986. Deep crustal structure and flexure of the Arabian plate beneath the Zagros collisional mountain belt as inferred from gravity observations. Tectonics 5, 361–373.

Sobouti, F., Arkani-Hamed, J., 1996. Numerical modelling of the deformation of the Iranian plateau. Geophys. J. Int. 126, 805–818.

Stephenson, R.A., Cloetingh, S.A.P.L., 1991. Some examples and mechanical aspects of continental lithospheric folding. Tectonophysics 188, 27–37.

Talbot, C.J., Alavi, M., 1996. In: The Past of a Future Syntaxis Across the Zagros. Geol. Soc. Spec. Publ. 100, 89–109..

Tapponnier, P., Molnar, P., 1976. Slip-line field theory and large scale continental tectonics. Nature 264, 319–324.

Tapponnier, P., 1977. Evolution tectonique du systeme alpin en Mediterranee: poincnnement et ecrasement rigide-plastique. Bull. Soc. Geol. Fr. 7, 437–460.

Tapponnier, P., 1978. Les mécanismes de la déformation intracontinentale: Example de la tectonique alpine en Asie et en Europe. Thèse de Doctorat d'Etat, Univ. Montpellier.

Tapponnier, P., Peltzer, G., Le Dain, A.Y., Armijo, R., Cobbold, P.R., 1982. Propagating extrusion tectonics in Asia: New insights from simple experiments with plasticine. Geology 10, 611–616.

Tchalenko, J.S., Braud, J., 1974. Seismicity and structure of the Zagros (Iran): The Main Recent Fault between 33° and 35°N. Philos. Trans. R. Soc. Lond. A 277, 1–25.

Truillet, R., Zargouni, F., Delteil, J., 1981. La tectonique tangentielle dans l'axe Nord–Sud (Tunisie centrale). C.R. Somm. Soc. Geol. Fr. 2, 50–54.

Turcotte, D.L., Schubert, G., 1982. Geodynamics Applications of Continuum Physics to Geological Problems. Wiley, New York.

Vermeer, P.A., 1990. The orientation of shear bands in biaxial tests. Geotechnique 40, 223–236.

Ward, S., 1994. Constraints on the seismotectonics of the central Mediterranean from very long baseline interferometry. Geophys. J. Int. 117, 441–452.

Wegener, A., 1912. Die Entstehung der Kontinente. Geologische Rundschau 3, 276–292.

Weijermars, R., 1986. Flow behaviour and physical chemistry of bouncing putties and related polymers in view of tectonic laboratory applications. Tectonophysics 124, 325–358.

Weijermars, R., Schmeling, H., 1986. Scaling of newtonian and non newtonian fluid dynamics without inertia for quantitative modelling of rock flow due to gravity (including the concept of rheological similarity). Phys. Earth Planet. Inter. 43, 316–330.

Zargouni, F., 1984. Style et chronologie des déformation des structures de l'Atlas tunisien méridionel. Actes 1er Congr. Nat. Sci. Terre, Tunis.

Zargouni, F., Abbés, C., 1985. The structural zonation of Tunisia. In: Galson, D.A., Mueller, S. (Eds.), European Geotraverse Project: the Southern Sector. European Science Foundation, Strasbourg.

Zhou, S., Sandiford, M., 1992. On the stability of isostatically compensated mountain belts. J. Geophys. Res. 97, 14207–14221.